INTERNATIONAL INSTITUTE
FOR
AERIAL SURVEY
AND
EARTH SCIENCES (ITC)
ENSCHEDE, THE NETHERLANDS

INVITED PAPER FOR COMMISSION IV

F. LEBERL

EVALUATION OF SINGLE STRIPS OF SIDE-LOOKING RADAR IMAGERY

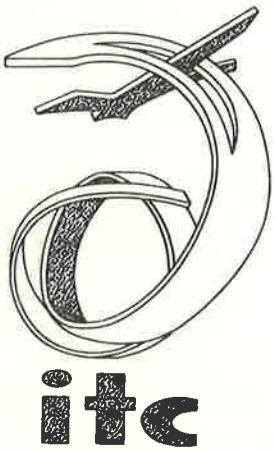

TWELFTH CONGRESS OF THE INTERNATIONAL SOCIETY FOR PHOTOGRAMMETRY. OTTAWA 1972

SUMMARY .

The metric evaluation of a single strip of side-looking radar-(SLAR-) imagery is the subject of the present paper, as a contribution to the discussion of ISP-Commission IV on "Metric Problems in Remote-Sensing". It stresses mainly theoretical considerations about the geometry of, and plotting from, a single strip of SLAR-imagery.

Starting from the projection equation, the functional model of SLAR is analyzed by going from the object area through the atmosphere, sensor platform and sensor to the imagery. Expressions for the effect of earth curvature and refraction are derived. A formula is given for the propagation of errors of the exterior orientation of the sensor into the imagery. The interior orientation is scrutinized, for the purpose of its calibration as well as analysis of possible error sources.

The stochastical model is based on the concept of random functions, since the imaging-process, unlike conventional photography, is time-dependent. The terrain as well as the exterior orientation can be described by their correlation functions. Propagating these into the imagery yields the stochastic model of image coordinates.

For the quantitative description of the characteristic properties of the SLAR-projection, the theory of TISSOT [76] is used and a number of numerical results computed.

The methods for plotting from a single strip of SLAR-imagery are described and classified according to whether or not they make use of the projection equations and their parameters, so that purely interpolative and parametric methods are obtained, as well as a combination of these two types. Further classification is possible according to whether the plotting is done numerically, photographically or graphically.

With actual imagery only the interpolative plotting methods have been tested, since no knowledge of the projection parameters was available. At check points, residual root mean square coordinate errors of $\pm$ 20 m to $\pm$ 60 m in across-flight direction, and $\pm$ 30 m to $\pm$ 80 m in flight-direction, were obtained, according to various strips of imagery, methods of plotting and distribution of control.

RÉSUMÉ .

L'évaluation pour des buts métriques d'une bande isolée d'images produites par radar à faisceau latéral (SLAR) est le sujet de ce rapport. Il représente une contribution à la discussion de la Commission IV du S.I.P. sur les "Problèmes Métriques de la Détection à Distance". On s'attache principalement aux considérations théoriques sur la géometrie et la restitution d'images par radar à faisceau latéral.

A partir des équations de projection on analyse le modèle fonctionel de l'image SLAR. En commençant par l'espace objet, en passant par l'atmosphère, la plateforme et finalement le senseur, on arrive à l'image même. On dérive des expressions pour l'effet de la courbure de la terre et la réfraction. La propagation des erreurs de l'orientation extérieure du senseur dans l'image est décrite par formules. L'orientation intérieure est analysée pour localiser des sources d'erreurs possibles et rendre possible leur calibration.

Le modèle stochastique est basé sur la théorie des fonctions aléatoires. C'est parce que le processus de formation de l'image s'étend dans le temps, au contraire de la photographie conventionelle. Le relief du terrain et l'orientation extérieure sont décrits à l'aide de leurs covariances. Les lois de propagation des covariances permettent de dériver le modèle stochastique de l'image.

Pour la description quantitative des propriétés caractéristiques de projection d'un système SLAR, on utilise la théorie de TISSOT. Un nombre d'exemples numériques a été calculé avec cette théorie.

Les méthodes de restitution de bandes isolées, qui sont décrites ci-après, peuvent être classifiées en méthodes d'interpolation, méthodes paramétriques et une combination de ces deux principes, selon qu'on utilise l'équation de projection ou non. Une autre classification est possible en accord avec l'application de méthodes de restitution numérique, photographique ou graphique.

Des résultats pratiques ont été seulement calculés pour les méthodes d'interpolation, parce que l'on a pas eu accès aux paramètres de projection des images qui étaient disponibles au cours de l'étude.

Les exemples numériques pour la restitution de bandes isolées ont produit des erreurs quadratiques moyennes dans les coordonnées de points de comparaison de $\pm$ 20 m à $\pm$ 60 m en travers, et $\pm$ 30 m à $\pm$ 80 m dans la direction de vol, en relation avec les méthodes de restitution, la distribution de points de controle et les diverses bandes d'image.

ZUSAMMENFASSUNG .

Die Auswertung einer einzelnen Radarschräg- (SLAR-) Aufnahme für metrische Zwecke ist das Thema der vorliegenden Arbeit, welche einen Beitrag zur Diskussion der Kommission IV der IGP über "Metrische Probleme der Fernerkundung" darstellt. Der Schwerpunkt liegt auf theoretischen Überlegungen über die Geometrie und Einzelbildauswertung von Radarschrägaufnahmen.

Ausgehend von der Projektionsgleichung wird das funktionale Modell der SLAR-Aufnahme analysiert, wobei vom Dingraum beginnend, über die Atmosphäre, den Träger des Aufnahmesystems und schliesslich den Sensor die Abbildung selbst behandelt wird. Ausdrücke für die Wirkung der Erdkrümmung und Refraktion werden abgeleitet. Die Fortpflanzung der Fehler der äusseren Orientierung des Sensors in die Abbildung wird formelmässig erfasst. Zum Zweck ihrer Kalibrierung wie auch der Analyse möglicher Fehlerquellen wird die innere Orientierung kritisch untersucht.

Das stochastische Modell beruht auf der Theorie der Zufallsfunktionen, denn der Abbildungsprozes ist im Gegensatz zur konventionellen Photographie zeitabhängig. Das Geländerelief wie auch die äussere Orientierung werden also mit Hilfe ihrer Kovarianzfunktionen beschrieben. Die Gesetze der Fehlerfortpflanzung ermöglichen es dann, das stochastische Modell der Abbildung herzuleiten.

Für die quantitative Beschreibung der charakterischen Abbildungseigenschaften des SLAR-Systems wird die TISSOTsche Theorie herangezogen. Eine Anzahl praktischer Zahlenbeispiele wurde hiermit berechnet.

Die Einzelbildauswertemethoden, welche im folgenden beschrieben und diskutiert werden, lassen sich in interpolative, parametrische und eine Kombination dieser gliedern, je nachdem, ob sie von den Projektionsgleichungen Gebrauch machen oder nicht. Eine weitere Gliederung ist schliesslich noch möglich entsprechend der Anwendung der Methode auf numerische, photographische oder graphische Art.

Praktische Ergebnisse werden nur für die interpolativen Verfahren ermittelt, da zum verfügbaren Bildmaterial keine Daten über irgendwelche Projektionsparameter vorhanden waren. In den numerischen Versuchen wurden in Vergleichspunkten mittlere Koordinatenfehler nach Einzelbildauswertung von etwa $\pm$ 20 m bis $\pm$ 60 m quer, und $\pm$ 30 m bis $\pm$ 80 m längs der Flugrichtung erhalten, entsprechend der Auswertemethode, Passpunktverteilung und verschiedenen Aufnahmen.

1. INTRODUCTION .

Radargrammetry as a part of - or as opposed to - photogrammetry has been accepted as research topic only two years ago by the International Society of Photogrammetry. On a national level, however, research in this field started much earlier. The earliest references which I could find concern a report of H.P. Smith, U.S.A., from 1948: "Mapping by Radar - The Procedures and Possibilities of a New and Revolutionary Method of Mapping and Charting", and an article by Prof. Dr. K. Rinner, Austria, prepared for the Austrian Academy of Science in 1948: "Die Geometrie des Funkmessbildes". This was thus 8 years after the first PPI-images were produced in England. A number of publications on PPI-evaluation appeared, before the concept of side-looking radar, developed since 1953, became known to the photogrammetric community. The possibility of mapping from radar was almost only considered in the U.S., as can be clearly seen from the literature at the end of this report. It was only at the last series of inter-congressional symposia in 1970 that the various ISP-commissions included the subject of remote-sensing in general and radar-mapping in particular into their programs and decided to devote a session during this congress to these subjects.

The photogrammetrist may be exposed to the problem of transferring radar data in a metrically correct way into a map coordinate system in the case where there is no timely photographic mapping alternative or whenever the photo-interpreter may request his service to transfer interpreted information onto a base map. These two tasks are different in the way that in the first case, ground control is scarce and in the second case it may not be. Another objective of plotting from SLAR-imagery may consist in the measurement of various derived metric quantities such as area, distances, angles and slope.

Logically, the first step in solving the task of plotting from SLAR is to consider a single strip of imagery. After construction of the geometrical model, the main difficulty to metrically evaluate SLAR- or other types of continuous strip imagery, stems from the dynamic mode of operation of the sensor system.

In a conventional aerial camera, the imaging parameters of interior and exterior orientation may be considered as random variables, whereas in the case of continuously imaging sensors, they become random functions. This increases considerably the complexity of the problem and prevents it from a rigorous solution. As a consequence the number of parameters describing a SLAR-strip metrically to a satisfactory extent is very large

and efforts to determine them are costly. Part of the present report will deal with these difficulties.

Another problem is the limited geometric resolution. The SLAR-image coordinates suffer from measuring errors due to lack of definition. Though the size of these errors can become considerable in commercially available imagery at present (2 - 40 m on the ground), it is expected that this range will be decreased in the near future with technological progress and declassification of military know-how to a size of 2 - 5 m. These last values will be obtainable at the expense of a loss of operational ease and reduced reliability.

In the following, the metric evaluation of SLAR-imagery as obtained from a non-coherent sensor will be surveyed. The results obtained are also valid for synthetic aperture or coherent radar, however with minor modifications. The presentation is based on results obtained in [29]. It is not considered necessary to repeat a basic description of the SLAR-sensor and its resolution capabilities. Instead, reference is made to the bibliography at the end of this report.

2. THE MATHEMATICAL MODEL .

The present study is concerned with the geometry of SLAR-imagery, and thus with the process of imaging the object space by means of the SLAR-projection onto the strip of imagery. This process will be mathematically modelled in the following.

The study is also concerned with the inverse of the above process, namely the reconstruction of the object space from SLAR-imagery. Since the mathematical model of the inverse is straightforward once it is known for the process of imaging, it is not derived separately in the following, but instead, additional remarks are given in the course of the discussion when considered necessary.

2.1. The Elements of the Functional Model.

Starting from the projection (or better imaging-) equations, its parameters can be investigated most logically by discussing first the effect of the object area, then going through the atmosphere, platform and sensor to the imagery.

2.1.1. The Projection Equation.

Figure 1 shows the coordinate systems referred to in the projection equation of SLAR. This equation states (Hockeborn [16]):

$$\underline{s} = \underline{A} \cdot \underline{B} \, (\underline{C} \cdot \underline{D} \cdot (\underline{X}_P - \underline{X}_F) + \Delta \underline{\bar{X}}) \qquad (1a)$$

or explicitely:

$$\begin{bmatrix} u \\ v \\ w \end{bmatrix}_s = \underline{A} \cdot \underline{B} \cdot (\underline{C} \cdot \underline{D} \cdot (\begin{bmatrix} X \\ Y \\ Z \end{bmatrix}_P - \begin{bmatrix} X \\ Y \\ Z \end{bmatrix}_F) + \begin{bmatrix} \Delta \bar{X} \\ \Delta \bar{Y} \\ \Delta \bar{Z} \end{bmatrix}) \qquad (1b)$$

and

$$\begin{bmatrix} u \\ v \\ w \end{bmatrix}_s = s \cdot \begin{bmatrix} \sin \Phi_o \\ (\cos^2 \Omega - \sin^2 \Phi_o)^{\frac{1}{2}} \\ \sin \Omega \end{bmatrix} \qquad (2)$$

In equation (1), $\underline{s}$ is the vector to the object point P in the coordinate system of the antenna (given by u,v,w) in figure 1 . The length of $\underline{s}$, namely s, is called "slant range". $\underline{X}_P$ defines the object point P and $\underline{X}_F$ the origin of the platform coordinate system as geocentric coordinates.

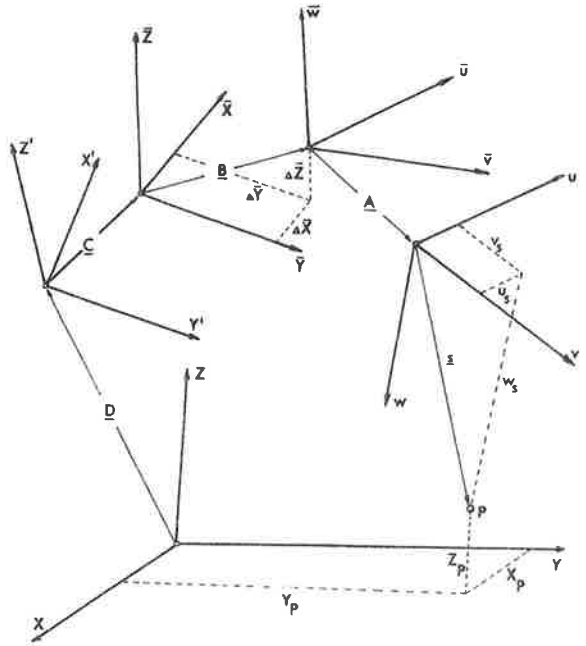

Figure 1.

Coordinate systems in the mathematical model of SLAR

$\Delta\ \underline{\bar{X}}$ is the position of the origin of the antenna-system in the platform coordinates $(\bar{X},\bar{Y},\bar{Z})$. $\underline{A}$, $\underline{B}$, $\underline{C}$ and $\underline{D}$ are orthogonal rotation matrices. In particular, $\underline{A}$ represents the rotation of the antenna-in the system of the antenna's fixation $(\bar{u},\bar{v},\bar{w})$ and is

$$\underline{A} = \begin{bmatrix} 1 & 0 & 0 \\ 0 & \cos\omega_o & -\sin\omega_o \\ 0 & -\sin\omega_o & -\cos\omega_o \end{bmatrix}$$

with ω_o as the angle between the v- and $\bar{v}$-coordinate axis.

$\underline{B}$ is the rotation matrix between the system of the antenna's mounting and the platform. As such it is a full matrix, of the same form as $\underline{C}$, which represents the orientation of the platform in the local rectangular system X', Y', Z', with Z' in the direction of the vertical and X' directed to the north:

$$\underline{C} = \begin{bmatrix} \cos\varphi.\cos\varkappa & \cos\varphi.\sin\varkappa & \sin\varphi \\ -\cos\omega.\sin\varkappa + \sin\varphi\cos\varkappa.\sin\omega & \cos\omega\cos\varkappa + \sin\varphi.\sin\omega\sin\varkappa & -\cos\varphi.\sin\omega \\ -\sin\varkappa.\sin\omega - \sin\varphi\cos\omega.\cos\varkappa & \sin\omega\cos\varkappa - \sin\varphi\sin\varkappa\cos\omega & \cos\varphi.\cos\omega \end{bmatrix}$$

Finally, D is the matrix of rotation from the X',Y',Z' - into the goecentric X,Y,Z-system and amounts to:

$$\underline{D} = \begin{bmatrix} \sin b.\cos l & \sin b.\sin l & \cos b \\ -\sin l & \cos l & 0 \\ -\cos b \cos l & -\cos b \sin l & -\sin b \end{bmatrix}$$

b, l are the geographical latitude and longitude, respectively.

In expression (2), then, the angle $\mathfrak{Q}$ is the depression angle of the "line of sight" or of the direction of $\underline{s}$, and Φ_o is the squint angle. This squint angle is present in some SLAR-sensors and is the complement to 90^o of the angle between the u-coordinate axis and $\underline{s}$. This means, that the radar signals do propagate along a cone of vertex angle $(180^o - 2 \cdot \Phi_o)$. $\Phi_o = 0$ cannot be achieved in systems with "endfeeding" of the antenna, where the energy is fed to the antenna from one of its ends.

The inverse of equation (1) would describe the process of reprojecting the SLAR-imagery into the object space.

2.1.2. Object Area.

The general formulation of the projection equation (1) is in three dimensional space, so that the shape of the earth-ellipsoid is taken into account. This case has specifically been considered in the Russian literature by Akowetzki [1], under some limiting assumptions for formulae (1), namely $\Phi_o = \Delta\underline{X} = 0$, $\underline{A} = \underline{B} = \underline{I}$ ($\underline{I}$ = unit matrix). The question arises, whether the eccentricity of the ellipsoid has a significant effect onto the SLAR-imagery, and inversely, whether it is necessary to account for this effect when plotting from SLAR.

This question can simply be answered; for example by assuming an object point P in the reference surface which is imaged by means of the SLAR-projection and then projected back onto a sphere. The discrepancies $(\Delta X_P, \Delta Y_P, \Delta Z_P)$ describe the effect of neglecting the ellipsoid's eccentricity. Table 1 shows the result of such a computation, where $\Delta r = (\Delta X_P^2 + \Delta Y_P^2 + \Delta Z_P^2)^{\frac{1}{2}}$ is given as a function of the latitude b, the flying height Z and the measured slant range s. This effect is much smaller than the neglection of the ellipsoid in the measurement and subsequent computation of the platform coordinates (X_F, Y_F, Z_F). In any case it is obvious, that it is not required to consider the ellipsoidal

shape of the Earth since the accuracy of the distance s as derived from the image coordinates is by far inferior to this effect.

b(°)	0		60	
z_F(km)	2	10	2	10
s=15 km	-0.1	-0.1	0	0
s=30 km	-0.4	-0.4	-0.1	-0.1

Table 1.

Effect Δ r (in m) of the eccentricity of the Earth's reference figure (geogr. longitude l = 0°, b = geogr. latitude).

A similar computation can answer the question, whether the spherical shape of the Earth is required in the projection-equation for SLAR. Figure 2 gives the Δ Y, and Δ Z, in a cartesian X, Y, Z-terrain coordinate system, with X parallel to the flight direction. ΔY_P, ΔZ_P represent the effect of earth curvature. From this figure it is seen, that the effect of earth curvature must be considered with certain accurate SLAR-systems.

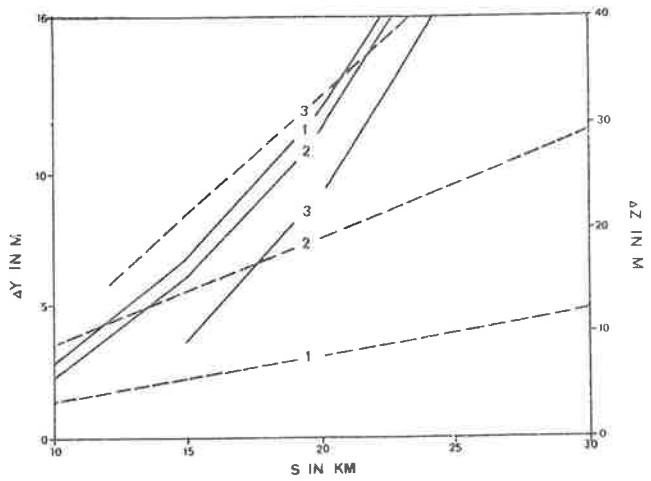

Fig. 2.

Effect of earth curvature on rectangular coordinates, derived from SLAR (1: Z_F = 2 km, 2: Z_F = 5 km, 3: Z_F = 10 km, —— ΔZ, - - - - ΔY).

For this purpose it is appropriate to correct the SLAR image-coordinates and to use subsequently a projection equation for a flat Earth rather than using the general formula (1). Figure 3 shows, how the measured entities have to be corrected for the curvature of the Earth. The corrections to be applied are such as if the object area would be transformed into an orthographic projection. To the slant range s is to be added :

$$\Delta_E s = s' - s = ((Z_P - Z_F)^2 + k^2))^{\frac{1}{2}} - s$$

$$\Delta_E s \approx - \frac{Z_P + Z_F}{2.R} \cdot s + \frac{(Z_F + Z_P) \cdot (Z_F - Z_P)^2}{2 \cdot R \cdot s} \qquad (3a)$$

and for ground range presentation:

$$\Delta_E s \approx - \frac{Z_F + Z_P}{2.R} \cdot y + \frac{(Z_P^2 - 2 Z_F \cdot Z_P)(Z_F + Z_P)}{2 \cdot R \cdot y} \qquad (3b)$$

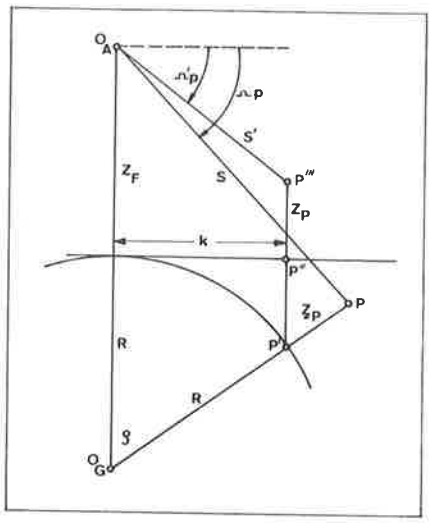

Fig. 3.

Geometry of SLAR and orthographic geodetic projection. O_A = sensor position, R = Earth radius.

Similarly, to the observed depression angle Ω one has to add:

$$\Delta_E \Omega \approx \sin (\Omega'_P - \Omega_P)$$

$$\Delta_E \Omega \approx \frac{- (Z_F^2 - Z_P^2 - s^2) \cdot (s^2 - (Z_F - Z_P)^2)^{\frac{1}{2}}}{2 \cdot R \cdot s^2} \qquad (4a)$$

and for ground range presentation:

$$\Delta_E \Omega \approx \frac{- (Z_P^2 + y^2) \cdot (y^2 - Z_P^2 + 2 \cdot Z_P \cdot Z_F)^{\frac{1}{2}}}{2 \cdot R \cdot (y^2 + Z_F^2)} \qquad (4b)$$

Table 2 gives some computed values for the function (3a). It can be shown, that the correction formulae for other reference projections, such as the equidistant cylindrical projection, are insignificantly different from (3) and (4).

s (km)	z_P (%z_F)	$\frac{-s(z_F-z_P)}{2R}$		$\frac{(z_F+z_P)(z_F-z_P)^2}{2Rs}$	
10	0	-1.6	-7.9	0.1	8.0
	30	-2.0	-10.2	0	5.1
15	0	-2.4	-11.8	0	5.2
	30	-3.1	-15.3	0	3.3
30	0	-4.7	-23.6	0	2.6
	30	-6.1	-30.7	0	1.6
z_F(km)		2	10	2	10

Table 2.

Corrections $\Delta_E s$ due to earth curvature (in m).

By applying these corrections (3) and (4), the projection formula (1) becomes simpler as the matrix $\underline{D}$ reduces to the unit matrix, and the geocentric system is replaced by a cartesian terrestrial (or model) system.

2.1.3. Atmosphere.

Electromagnetic radiation of the SLAR-system - as with any kind of electronic distance measurement - does not propagate rectilinearly, but is refracted due to the changing refractive index of the atmosphere. The resulting electro-magnetic path can be approximated by a circle. When plotting from SLAR, then the following corrections to the measured entities must be considered due to refraction:

- curvature correction,
- velocity correction.

The radius of curvature, r, of the radiation path is approximated by Laurila [70], as:

$$\frac{1}{r} = i + j.(Z_P + Z_F) - \frac{j}{6} s^2.(\frac{1}{R} + i + j(Z_F + Z_P));$$

$$i = -3.7 . 10^{-5}$$

$$j = 1.4 . 10^{-6}$$

The effects on s and Ω are:

$$\Delta_n s = \frac{s^3}{24.r^2} \qquad \Delta_n \Omega = 90. s / (r.\pi)$$

Figure 4 demonstrates that the curvature correction is negligible.

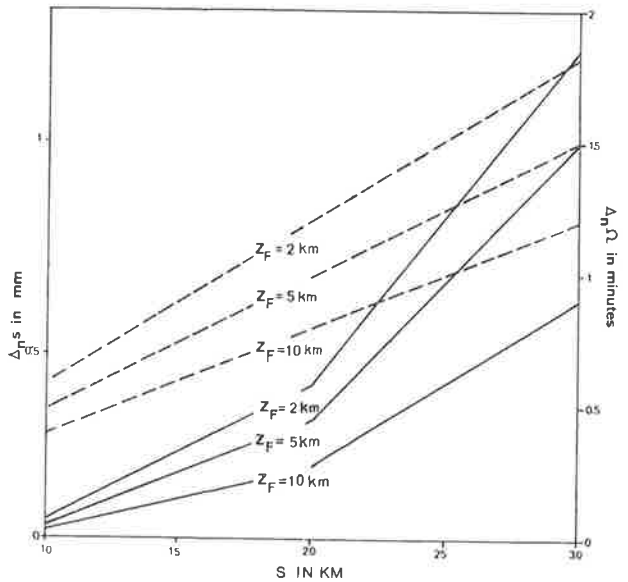

Fig. 4.

Correction due to curvature of electromagnetic path
(——— $\Delta_n s$, ------ $\Delta_n \Omega$)

The velocity-correction for s results from the difference Δ r between the actual refractive index and the one used for converting echotime into s. This correction

$$\Delta_r s = -\frac{s}{r} \cdot \Delta r$$

is plotted in figure 5. Only in cases where one uses a refractive index of 1, such correction could be significant.

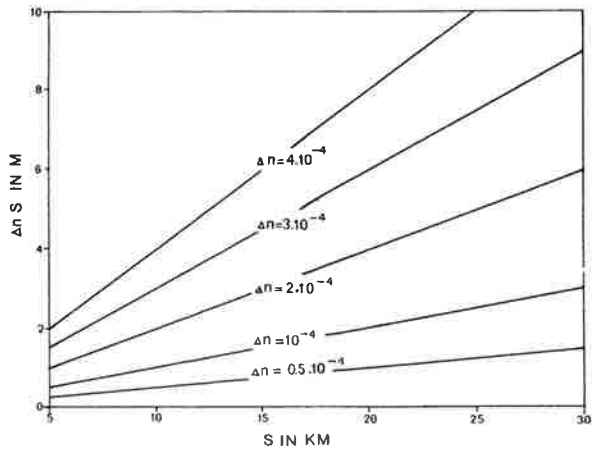

Fig. 5.

Velocity correction due to erroneous refractive index.

2.1.4. Exterior orientation.

Due to the deviation of the sensor, i.e. the antenna, from a rectilinear, horizontal movement with constant speed and orientation equal to $\varphi = \omega = \varkappa = 0^{\circ}$, the entities as measured in the object space differ from the ideal value. These differences and their effect onto the image coordinates cannot be described only by the partial differential of the projection equation, since it would only result in an error vector $\underline{ds}$, which, in general, may not completely describe the effect on the image-coordinates x and y. Therefore, another approach is followed.

Defining the x,y-image-coordinates as in section 2.1.6., namely y to be proportional to the slant range s and x to the time at which an object point was imaged, one can formulate from fig. 6 the following definition of image displacements due to an erroneous exterior orientation.

$$\Delta y = \bar{y} - y = \left((X_P - \bar{X}_F)^2 + (Y_P - \bar{Y}_F)^2 + (Z_P - \bar{Z}_F)^2 \right)^{\frac{1}{2}} - \left((X_P - X_F)^2 + (Y_P - Y_F)^2 + (Z_P - Z_F)^2 \right)^{\frac{1}{2}} \quad (5a)$$

$$\Delta x = \bar{a} - a - (a / v_F) \cdot \Delta v_F \quad (5b)$$

where

$$a = \left((\bar{X}_F - X_F)^2 + (\bar{Y}_F - Y_F)^2 + (\bar{Z}_F - Z_F)^2 \right)^{\frac{1}{2}}$$

$$\bar{a} = \int_{t_o}^{t_p} \left(\dot{X}^2(t) + \dot{Y}^2(t) + \dot{Z}^2(t) \right)^{\frac{1}{2}} dt$$

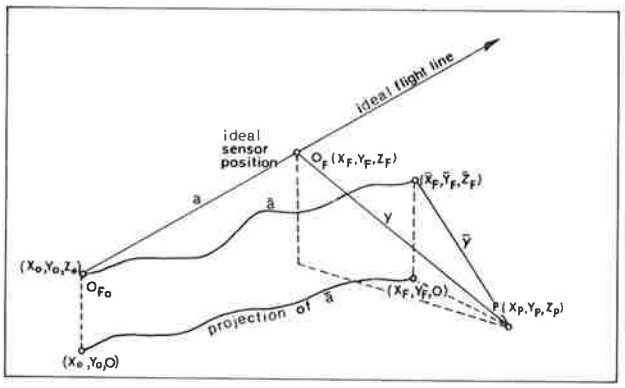

Fig. 6.

Image displacement due to erroneous exterior orientation.

$\dot{X}(t)$, $\dot{Y}(t)$, $\dot{Z}(t)$ are the first time-derivative of the parametric form of the flight path, Δv_F the error in the speed of the film travel. Obviously, Δy is given as function of $X_F - \bar{X}_F$, $Y_F - \bar{Y}_F$, $Z_F - \bar{Z}_F$ and the coordinates of point P, whereas Δx incorporates the whole history of the platform-speed and path.

To derive expressions for image displacements, we start from the assumption, that $\bar{a}$ of fig. 6 is rectilinear and makes a horizontal angle α with the ideal flight line and an angle β with the horizontal.

Then:

$$\begin{bmatrix} \bar{X}_F \\ \bar{Y}_F \\ \bar{Z}_F \end{bmatrix} = \bar{a} \begin{bmatrix} \cos\beta \cdot \cos\alpha \\ \cos\beta \cdot \sin\alpha \\ \sin\beta \end{bmatrix} + \begin{bmatrix} 0 \\ 0 \\ Z_F \end{bmatrix}$$

From the projection equation (1) with $\underline{A} = \underline{B} = \underline{I}$, $\Phi_o = 0$, $\bar{a}$ can be found as a function of $\Delta\varphi$, $\Delta\omega$, $\Delta\kappa$, X_P, Y_P, Z_P, Z_F. Introducing this $\bar{a}$ into equation (5b), linearizing and neglecting all terms of higher than first order gives:

$$\Delta x \approx - X_P \cdot \Delta v_F / v_F + Y_P \Delta\kappa + (Z_P - Z_F)\,\Delta\varphi$$

$$\Delta y \approx - Y_P \cdot (\bar{a} \cdot \alpha) / y + (Z_F - Z_P) \cdot (\bar{a} \cdot \beta) / y$$

Substituting now $\bar{a} \cdot \beta = \Delta Z_F$, $\bar{a} \cdot \alpha = \Delta Y_F$, and setting $Z_P = 0$, one obtains

$$\begin{aligned} \Delta x &\approx - \Delta X_F + Y \cdot \Delta\kappa - Z_F \Delta\varphi \\ \Delta y &\approx - (Y/y) \cdot \Delta Y_F + (Z_F/y) \cdot \Delta Z_F \end{aligned} \qquad (6a)$$

This is the formula obtained in [27] by a different derivation and gives the first order effects of errors in exterior orientation on to the image coordinates x and y. It should be noted, that the erroneous attitude of the sensor has no effect on Δy !

Considering the inverse, namely the use of erroneous data of exterior orientation for plotting from a single strip of imagery, then one obtains the errors in ground coordinates, ΔX_P, ΔY_P, assuming $Z_P = 0$, as:

$$\begin{aligned} \Delta X_P &\approx + \Delta X_F - v_s \cdot \Delta\kappa + w_s \cdot \Delta\varphi \\ \Delta Y_P &\approx \Delta Y_F - \frac{w_s}{v_s} \cdot \Delta Z_F \end{aligned} \qquad (6b)$$

Here, v_s and w_s are two components of the range vector $\underline{s}$ (see equ. (1)).

2.1.5. Interior Orientation.

Interior orientation is defined as the relation between the measured entity in the object space and its analog in the image space. To study the interior orientation and its error sources, it is appropriate to consider the components of a SLAR-system in general and of its recording unit in particular (see fig. 7a, 7b).

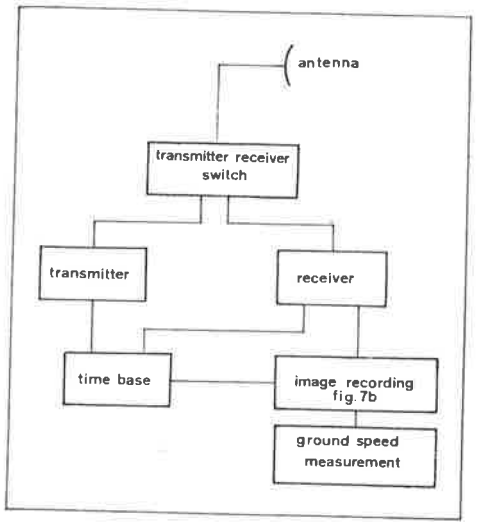

(a)

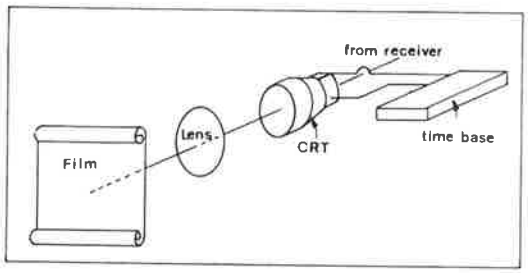

(b)

Fig. 7.

Interior orientation:
(a) components of SLAR-system,
(b) image recording unit of SLAR-system

The components,which determine the inner orientation, are:

- the antenna
- the time-basis
- the sensor for the ground speed
- the CRT
- the optical system
- the film
- the film transport.

The following errors of the inner orientation are feasible and can be put into an algebraic form:

Time-basis: The "sweep delay" d_o, which is the time between transmission of the impulse and the beginning of registration of the echos, could be erroneous by Δd_o. So the y-coordinates would have an error of:

$$\Delta y = c_F \cdot \Delta d_o \quad ,$$

where c_F is the velocity of the flying spot of the CRT.

CRT: The voltage in the CRT should be such as to make the flying spot move with a constant (if slant-range) or other given speed (if ground range presentation). Any deviation of the required voltage causes an error Δy. On the other hand, the CRT-screen is not flat, but curved (see fig. 8). This curvature, together with the effect of "fringe-fields" perturbing the magnetic CRT-field, has effects that have been described by Wong [78] with the help of two polynomials:

$$\Delta x = -y \cdot (q_1 \cdot |r| + q_2 |r^3| + \dots)$$

$$r = (y - y_{max})/2$$

$$\Delta y = y \cdot (p_1 + p_2 r^2 + \dots)$$

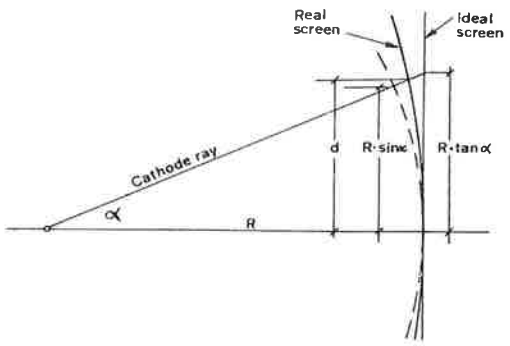

Fig. 8.

Deviation of cathode ray, $R \sin \alpha < d < R \tan \alpha$

Optical system: There is distortion with an effect similar to the one of "fringe-fields" and to be corrected with the same formula. The error Δf in the focal distance produces a scale error in y-direction. Erroneous coordinates of the projection centre lead to constant errors (Δx_o, Δy_o). If the orientation of the optical axis is not adjusted, then this produces only a defect in definition, but not a geometric error, so that:

$$\Delta x = \Delta x_o ,$$

$$\Delta y = \Delta y_o + \frac{y}{f} \cdot \Delta f$$

Film: In the case when the x-axis is not perpendicular to the optical axis, an error similar to a $\Delta\varphi$-error of exterior orientation is produced. The y-axis, if not properly perpendicular to the optical axis, produces a $\Delta\omega$-error. There is the possibility of the x-axis not being normal to the path of the flying spot. This corresponds to an error of $\varkappa$ (see Konecny & Derenyi [67]). As a result:

$$\Delta x = f \cdot \Delta\bar{\varphi} + y \cdot \Delta\bar{\varkappa}$$

$$\Delta y = \frac{r^2 + f^2}{f} \cdot \Delta\bar{\omega}$$

Film transport and measurement of ground-speed: In a synchronized system, the measured ground speed requires a certain film velocity. This synchronization can be achieved by a servomotor, with eventually limited accuracy. One could conclude that in a SLAR-survey for metric evaluation of the imagery, a constant film speed is superior, since the error of synchronization is avoided and the data on the aircraft speed can be recorded on tape. But if an error Δv_F of film speed is present, it produces:

$$\Delta x = x \cdot \Delta v_F / v_F$$

Considering the accuracy of measuring the ground speed, the following can be said: since this measurement is of a relative accuracy in the order of 1/1000, it is sufficient for a cartographic SLAR-system. Long term error trends can be controlled by a few control points.

The formula resulting from the above for the description of the errors of interior orientation is then:

$$\Delta x_{total} = \Delta x_o + f \cdot \Delta\bar{\varphi} + y \cdot \Delta\bar{\varkappa} + \frac{x}{v_F}\Delta v_F - y \cdot (q_1 |r| + q_2 |r^3| + \ldots)$$

$$\Delta y_{total} = \Delta y_o + \frac{y}{f} \cdot \Delta f + \frac{r^2 + f^2}{f} \cdot \Delta\bar{\omega} + y \cdot (p_1 + p_2 r^2 + \ldots)$$

Some of the coefficients in this formula are time functions. No quantitative information is available to the author to test the significance of the derived expression.

2.1.6. Image Coordinates.

Equation 1 does not contain the raw output of a SLAR-survey, namely image-coordinates. For plotting, these have to be converted to the the entities appearing in equation 1.

The coordinate system in the imagery is defined so that the y-axis is in the direction of the movement of the flying spot of the CRT. The x-direction is perpendicular and opposite to the direction of film transport.

The y-coordinate of an image-point P', in the case of "slant-range-recording", is proportional to the distance between the object point P and the electrical centre of the antenna. So:

$$y_s = c_F \cdot (2.s/c_m - d_o) \qquad (7a)$$

In (7), c_F is the velocity of the electromagnetic impulse, c_m the speed of the flying spot on the CRT-screen, s the slant range and d_o the so-called "sweep-delay".

"Ground-range-presentation" reduces the slant range into "ground-range", i.e. a distance proportional to the orthogonal projection of the range vector. With k as a scale factor:

$$y_G = k \cdot ((s^2 - Z_F^2)^{\frac{1}{2}} - (d_o^2 c_m^2 / 4 - Z_F^2)^{\frac{1}{2}}) \qquad (7b)$$

For the purpose of plotting it is obvious that the scalar s, required in formula (2) for the definition of the range-vector $\underline{s}$, has to be computed from (7a, 7b), when the y-image coordinate is measured.

The x-coordinate of an image-point P' is a function x (t) of the time t at which the object point P has been imaged. If t_o is the time, for which x = 0, and t_P the time at which $x = x_P$, then:

$$x_P = \int_{t_o}^{t_P} v_F (t) \, d t \qquad (7c)$$

with v_F as the velocity of the film.

If the film transport is constant, then:

$$x_P = k. \int_{t_o}^{t_P} w(t).v_G\,(w(t)\,)\,dt = v_F.(t_P - t_o)$$

where v_G is the aircraft ground speed, and w(t) the path of the aircraft.

A film transport that is synchronized with the aircraft ground speed results in:

$$x_P = k. \int_{t_o}^{t_P} \bar{w}\,(t)\,dt$$

with $\bar{w}(t)$ as the aircraft ground track.

Usually the x_P-coordinate can, for plotting purposes, be directly used to relate the recorded data of exterior orientation to the image-point P'. In the more general case, however, we could consider the problem of determining t_P from the given x_P and to enter with t_P into the file of navigational data to derive from that position and orientation of the sensor at the time of imaging P.

2.1.7. Viewing Geometry and Relief Displacement.

Image displacements occurring in a SLAR-system even with ideal orientation are inherent to the system (figure 9) and consist of the well known typical SLAR-image deformations. For the sake of completeness, they are described separately here:

$$\Delta x = 0$$

$$\Delta y = Y_P - (Y_P^2 + (Z_F - Z_P)^2\,)^{\frac{1}{2}} + Z_F \qquad \text{(slant-range presentation)}$$

$$\Delta y = Y_P - (Y_P^2 + (Z_F - Z_P)^2 - Z_F^2)^{\frac{1}{2}} \qquad \text{(ground-range presentation)}$$

For $Y_P > (Z_F - Z_P)$, the expressions become:

$$\Delta y \approx (Z_F - \frac{Z_F^2}{2Y_P}) + \frac{2Z_FZ_P - Z_P^2}{2Y_P} \qquad \text{(slant-range)} \quad (8a)$$

$$\Delta y \approx \frac{-Z_P^2 + 2Z_FZ_P}{2Y_P} \qquad \text{(ground-range)} \quad (8b)$$

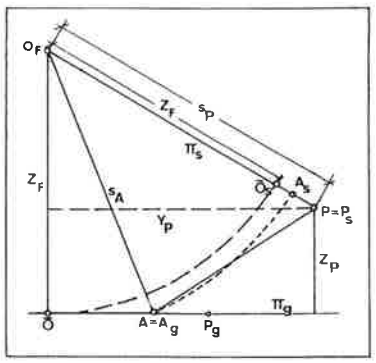

Fig. 9.

Viewing geometry with SLAR. π_s = projection plane for ground range presentation, π_g = projection plane for slant range presentation. AP = slope, $A_s P_s$ = image of slope in slant range presentation, $A_g P_g$ = image of slope in ground range presentation.

In formula (8a), the first term denotes the well-known SLAR-image deformation in slant range presentation; the last one the relief displacement. As can be seen from (8b), ground range presentation only shows relief displacement. There it can not be seen, that relief-displacement is slightly larger in the ground than in the slant range presentation. This is obviously caused by the fact that the slant range presentation compensates partly for the effect of relief. The formula to correct the relief displacement in ground range presentation is given in (8b). To correct this effect in the slant range presentation so as to obtain the pure slant range deformation, the formula

$$\Delta y = \frac{2 Z_F Z_P - Z_P^2}{2.s} \qquad (8c)$$

would have to be applied. Here the difference of relief displacements in the two imaging modes becomes obvious, since $s > Y_P$.

Squint.

The conical shape of the radar impulses due to the eventually present squint angle Φ_o is illustrated in figure 10. For the assumptions concerning coordinate systems and orientation as given in this figure, one can write:

$$\cot \Phi_o \cdot X_P = (Y_P^2 + (Z_P - Z_F)^2)^{\frac{1}{2}}$$

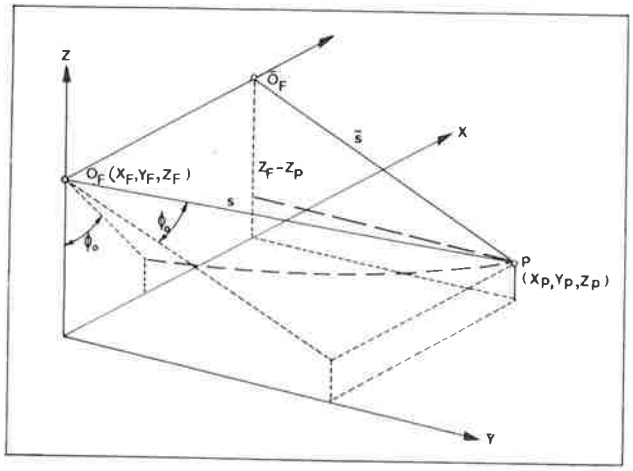

Fig. 10.
Effect of squint angle Φ_o.

This gives then:

$$\Delta x = X_P = \tan \Phi_o . \bar{s} = \sin \Phi_o . s$$

Denoting with $\bar{s}$ the slant range as measured without squint, and defining $\Delta y = s - \bar{s}$ for a slant range projection, one obtains:

$$\Delta y = s - s. \cos \Phi_o \approx s. \Phi_o^2 / 2$$

In the case of ground range presentation, one has

$$\Delta y = y - \bar{y} = y - ((s - s.\Phi_o^2 / 2)^2 - Z_F^2)^{\frac{1}{2}}$$

$$\Delta y \approx y - (y^2 - (y^2 + Z_F^2) . \Phi_o^2)^{\frac{1}{2}}$$

$$\Delta y \approx s^2 . \Phi_o^2 / (2.y)$$

In this presentation mode, the flying height influences the effect of the squint on the y-coordinates. For $Y_P = Z_F . \cos \Phi_o$, Δy has a maximum.

2.2. The Stochastical Model.

The continuous SLAR-imagery (and other types of dynamic imagery) are produced in a process which extends in time. The dependency on time is

an integral part of the character of the phenomena involved with dynamic imagery. So some of the parameters which - for conventional frame photography - might be considered to be random variables, are random functions in the case of dynamic imagery. This concept of random functions is now starting to enter also the field of conventional photogrammetry, by using it for the description of lens deformations, film shrinkage and digital terrain models. In the following, it will be used to analyze the stochastic properties of the SLAR-imagery. To this end, the exterior orientation and the object of a SLAR-survey, the terrain, are studied with respect to the concept of random functions. For basic definitions reference is made to the extensive literature on stochastic processes, e.g. Yaglom [79] .

2.2.1. Object Area.

Terrain relief can be interpreted as the realization of a one-dimensional stochastic field on the XY-terrain coordinate plane. This random field, Z (X,Y), consists of one random variable at each point (X,Y) of the reference space. The correlation function of a field in general has then four independent variables:

$$\text{Cov}\ (X_1, Y_1, X_2, Y_2) = q\ (X_1, Y_1, X_2, Y_2) =$$

$$= E\{ Z(X_1, Y_1) \cdot Z(X_2, Y_2) \}$$

$$X_2 = X_1 + \Delta X, \quad Y_2 = Y_1 + \Delta Y ;$$

where $E\{ . \}$ denotes statistical expectation.

In a "homogeneous, isotropic" field*, however, the correlation function is invariant under translation and rotation, so that the correlation function is only a function of the distance $(\Delta X^2 + \Delta Y^2)^{\frac{1}{2}}$.

In order to be able to assume homogeneity (= a.o. constant mean) for terrain, a trend has to be subtracted from the measured data. This can be done by a two dimensional moving average. (For an explanation of moving averages, see section 4.2.2.). Assuming isotropy, it is only necessary

---

*) A stochastic field is said to be homogeneous, if its mean value $E\{ Z(X,Y)\}$ is a constant and if its correlation function $E\{ Z(X_1,Y_1) \cdot Z(X_2,Y_2) \}$ only depends on the vector P_1P_2, $P_1 = (X_1,Y_1)$, $P_2 = (X_2,Y_2)$ (invariant under translation).

A stochastic field is said to be isotropic, if its correlation function depends only on the length of the vector P_1P_2, but not on its direction (invariant under rotation).

to consider a profile rather than a two-dimensionally extended sample of terrain to compute its covariance. An example is given in figure 11. The correlation functions for these data are given in figures 12a and 12b.

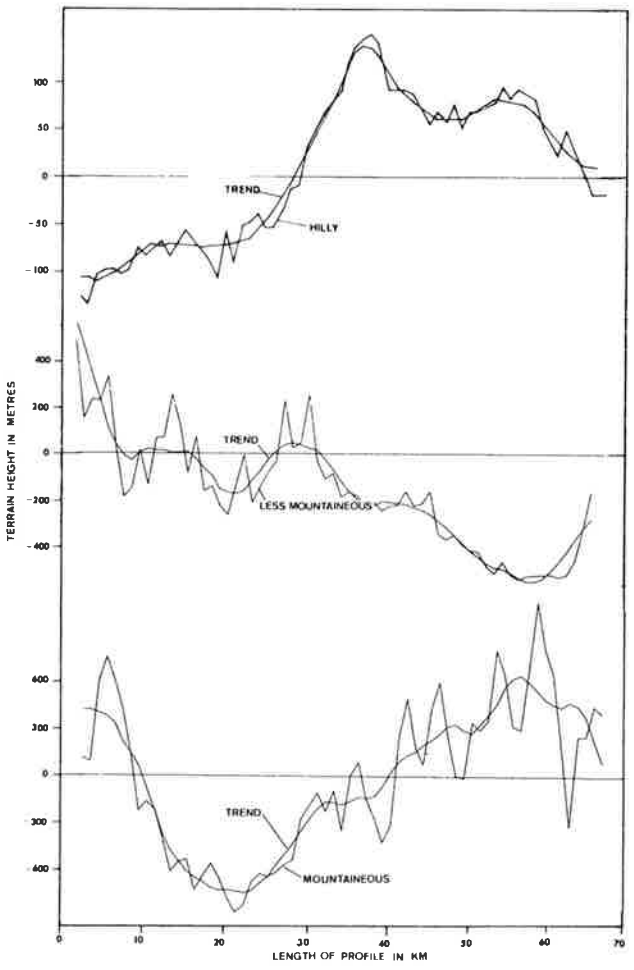

Fig. 11.
Profiles measured in hilly (Limburg, Netherlands), less mountainous and mountainous areas (Switzerland). The values are reduced for the average height. Trend computed with moving average.

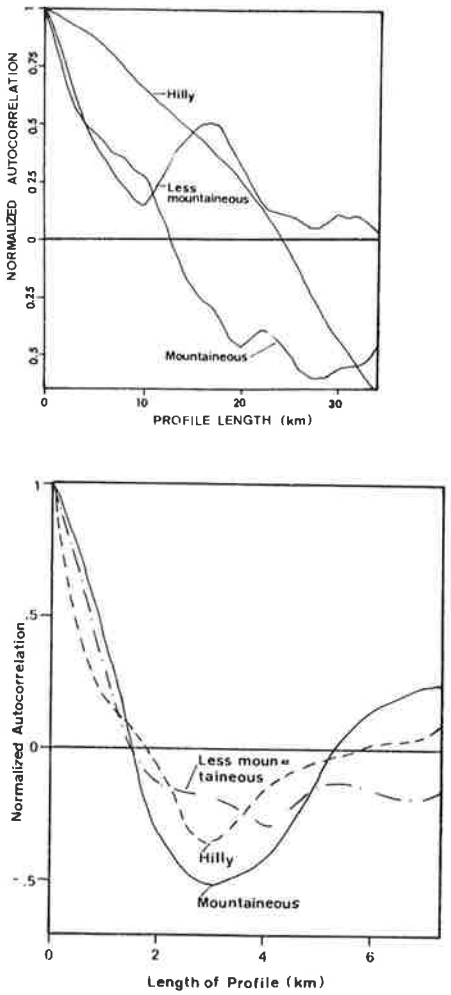

Fig. 12.
Normalized autocorrelations of data given in fig. 11, namely:
(a) of raw data, and
(b) of residuals after subtracting a trend.

Due to the assumption of stationarity, matrix $\underline{Q}$ is symmetrical, since

$$q_{\varphi,\omega}(\Delta t) = E\{\varphi(t) \cdot \omega(t + \Delta t)\} =$$
$$= E\{\varphi(t + \Delta t) \cdot \omega(t)\} = q_{\omega,\varphi}(\Delta t)$$

2.2.3. Image Coordinates.

The effect of erroneous elements of exterior orientation on the SLAR-image coordinates was given in formula (6a). Together with the expression for the relief displacement from equation (8c), with the second order term $Z_P^2 / 2s \approx 0$, this is repeated for easier reference:

$$\begin{aligned} \Delta x &= -\Delta X_F + (y^2 - Z_F^2)^{\frac{1}{2}} \Delta\varkappa - Z_F \cdot \Delta\varphi \\ \Delta y &= -\left((y^2 - Z_F^2)^{\frac{1}{2}} / y \right) \Delta Y_F + (Z_F / y) \Delta Z_F - \\ &\quad - (Z_F / (y^2 - Z_F^2)^{\frac{1}{2}}) Z_P \end{aligned} \qquad (12)$$

From this* equation (12) the correlation-functions of the image coordinates,

$$q_{\Delta x, \Delta x},\ q_{\Delta y, \Delta y},\ q_{\Delta x, \Delta y}$$

can be computed as a function of the correlations of the elements of exterior orientation, ΔX_F, ΔY_F, ΔZ_F, $\Delta\varphi$, $\Delta\varkappa$, and of the correlation of the relief. To every image-point (x, y) there belong in this way two stochastic variables (Δx, Δy), so that the imagery can be interpreted as a two-dimensional (due to Δx, Δy) stochastic field on the two-dimensional reference surface given by (x, y).

The computation of the correlation functions of Δx, Δy would be simpler, if the functions in (12) are stochastically linear. This is the case when assuming that y and Z_F are deterministic entities (i.e. non-stochastic). Then, the auto- and cross-covariances of Δx and Δy result from:

$$q_{\Delta x, \Delta x}(\underline{r}_1, \underline{r}_2) = E\{\Delta x(\underline{r}_1) \cdot \Delta x(\underline{r}_2)\}$$

$$q_{\Delta y, \Delta y}(\underline{r}_1, \underline{r}_2) = E\{\Delta y(\underline{r}_1) \cdot \Delta y(\underline{r}_2)\}$$

$$q_{\Delta x, \Delta y}(\underline{r}_1, \underline{r}_2) = E\{\Delta x(\underline{r}_1) \cdot \Delta y(\underline{r}_2)\}$$

with $\underline{r}_1 = (x_1, y_1)$, $\underline{r}_2 = (x_2, y_2)$

---

*) The image coordinate y is assumed to be equal to the slant range s.

with $\underline{m}$ (t) a vector of "trends" or means and $\underline{g}$ (t) the vector of stochastic components. This means that each element of the exterior orientation is considered to be composed of a trend-function or variable mean and a superimposed stochastic component. This assumption is rather arbitrary, since actually the total $\underline{f}$ (t) is a stochastic entity; on the other hand, a separation as proposed above will allow the rules for stationary functions to be applied to $\underline{g}$ (t), whereas $\underline{f}$ (t) certainly is not stationary at all.

When measuring $\underline{f}$ (t), a measuring error $\underline{e}$ (t) occurs, so that (9) becomes

$$\underline{f}' (t) = \underline{m} (t) + \underline{g} (t) + \underline{e} (t) = \underline{f} (t) + \underline{e} (t) \qquad (10)$$

To fulfil the theoretical requirement of stationarity, the "trend" $\underline{m}$(t) has to be eliminated in (10), so that further considerations are concentrated on: $\underline{f}'$ (t) - $\underline{m}$ (t). We introduce

$$\underline{f}' (t) - \underline{m} (t) = \underline{g} (t) + \underline{e} (t) = \underline{h} (t) \qquad (11)$$

The description of the stochastic properties of a stationary, normally distributed random function is complete by giving the correlation-function $q(t, \Delta t)$ (= $q(\Delta t)$, since stationarity implies independence of the correlation-function from t !).

This correlation-function is defined for a single process as

$$q (t, \Delta t) = q(\Delta t) = E \{ f (t) \cdot f (t + \Delta t) \}$$

For the vector process of exterior orientation, a matrix $\underline{Q}$ of correlation-functions is defined: each element of the matrix is a correlation function:

$$\underline{Q}_{6,6} = \begin{bmatrix} q_{\varphi\varphi}(\Delta t), & q_{\varphi,\omega}(\Delta t) & \cdots & q_{\varphi, Z_F}(\Delta t) \\ q_{\omega,\varphi}(\Delta t), & q_{\omega,\omega}(\Delta t) & \cdots & q_{\omega, Z_F}(\Delta t) \\ \cdots & \cdots & \cdots & \cdots \\ q_{Z_F,\varphi}(\Delta t), & q_{Z_F,\varphi}(\Delta t) & \cdots & q_{Z_F,Z_F}(\Delta t) \end{bmatrix}$$

The off-diagonal elements are cross-correlations, e.g.:

$$q_{\varphi,\omega}(\Delta t) = E \{ \varphi(t) \cdot \omega (t + \Delta t) \}$$

Substitution of (12) in this set of equations gives then:

$$q_{\Delta x, \Delta x}(\underline{r}_1, \underline{r}_2) = (y_1^2 - Z_F^2)(y_2^2 - Z_F^2)^{\frac{1}{2}} \cdot q_{\varkappa,\varkappa}(x_2 - x_1) +$$

$$+ Z_F^2 \cdot q_{\varphi,\varphi}(x_2 - x_1) + q_{\Delta X, \Delta X}(x_2 - x_1) -$$

$$- (y_2^2 - Z_F^2)^{\frac{1}{2}} \cdot (Z_F \cdot q_{\varphi,\varkappa}(x_2 - x_1) +$$

$$+ q_{\varkappa, \Delta X}(x_2 - x_1)) + Z_F \cdot q_{\varphi, \Delta x}(x_2 - x_1)$$

and similar expressions for $q_{\Delta y, \Delta y}$, $q_{\Delta x, \Delta y}$. Since the correlations due to exterior orientation depend on x and y and not only on $[(x_2 - x_1)^2 + (y_2 - y_1)^2]^{\frac{1}{2}}$, it is proved, that the coordinate-errors Δx, Δy do form an inhomogeneous, anisotropic stochastic field (of which the correlation functions are variable with translation and rotation).

The propagation of the correlations of the errors of exterior orientation into the terrain coordinates can be derived analogously from equations (6b).

3. APPLICATION OF THE THEORY OF TISSOT TO THE SLAR-PROJECTION.

Characteristic properties of a projection are described in cartography by means of the theory of TISSOT, in which the deformation of distances, angles or directions, and areas are investigated [76] . For this purpose, differentially small units are used.

3.1. Definitions.

The application of the theory is based on the imaging equations, thus the inverse of formula (1), so that one can write:

$$x_P = h' (X_P, Y_P, Z_P) = h (X_P, Y_P)$$

$$y_P = g' (X_P, Y_P, Z_P) = g (X_P, Y_P)$$

where Z_P is considered a function of X_P and Y_P.

According to figure 13a:

$$dl = (dX^2 + dY^2 + dZ^2)^{\frac{1}{2}}$$

Projection of dl into the XY-plane gives:

$$dl'' = (dX^2 + dY^2)^{\frac{1}{2}}$$

In the imagery, there occurs (fig. 13b):

$$dl' = (dx^2 + dy^2)^{\frac{1}{2}} \qquad (13)$$

Because of

$$dx = \frac{\delta h}{\delta X} dX + \frac{\delta h}{\delta Y} dY = \left(\frac{\delta h}{\delta X} + \frac{\delta h}{\delta Y} \tan \gamma \right) dX$$

$$dy = \frac{\delta g}{\delta X} dX + \frac{\delta g}{\delta Y} dY = \left(\frac{\delta g}{\delta X} + \frac{\delta g}{\delta Y} \tan \gamma \right) dX$$

formula (13) becomes:

$$dl'^2 = I \cdot dX^2 + J \cdot dY^2 + K \cdot dX \cdot dY.$$

$$I = \left(\frac{\delta h}{\delta X} \right)^2 + \left(\frac{\delta g}{\delta X} \right)^2; \quad J = \left(\frac{\delta h}{\delta Y} \right)^2 + \left(\frac{\delta g}{\delta Y} \right)^2; \quad K = 2. \left(\frac{\delta h. \delta h}{\delta X. \delta Y} + \frac{\delta g. \delta g}{\delta X. \delta Y} \right)$$

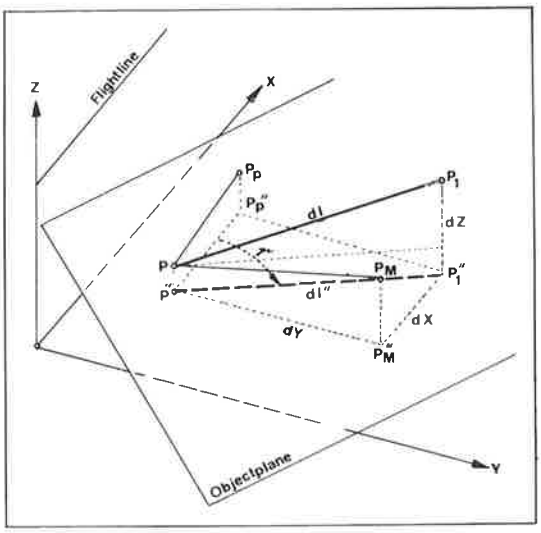

Fig. 13.

Definitions (a) in object space and
(b) in image space
for application of Tissot's Theory.

Denoting the direction of dl" in the XY-plane by γ, and the respective direction in image space with γ', one can write:

$$\cos \gamma' = \frac{dx}{dl'}, \qquad \sin \gamma' = \frac{dy}{dl'},$$

$$\tan \gamma' = \frac{\frac{\delta g}{\delta X} + \frac{\delta g}{\delta Y} \cdot \tan \gamma}{\frac{\delta h}{\delta X} + \frac{\delta h}{\delta Y} \cdot \tan \gamma}$$

A differential surface element dF' in image space is, from figure 13b:

$$dF' = P'P'_P \cdot P'P'_M \cdot \sin (\gamma'_M - \gamma'_P)$$

$$= (I.J)^{\frac{1}{2}} \cdot dX \cdot dY \cdot (\sin\gamma'_M \cdot \cos \gamma'_P - \cos \gamma'_M \cdot \sin \gamma'_P)$$

This can be simplified to:

$$dF' = \left(\frac{\delta h}{\delta X} \cdot \frac{\delta g}{\delta Y} - \frac{\delta h}{\delta Y} \cdot \frac{\delta g}{\delta X}\right) dX. dY = G. dX.dY$$

With the above definitions, the distance-, angle-, and surface-deformation can be derived.

The distance-deformation τ is

$$\tau = \frac{dl'}{dl''}$$

$$\tau^2 = I.\cos^2\gamma + J.\sin^2\gamma + (K/2).\sin 2\gamma$$

The angle-deformation μ (as opposed to the original "direction-deformation" of TISSOT) is:

$$\mu = \gamma_1' - \gamma_2' + \gamma_2 - \gamma_2 = \gamma_{12}' - \gamma_{12}$$

$$\mu = \frac{G.(\tan\gamma_1 - \tan\gamma_2) - \tan(\gamma_1 - \gamma_2)(I + J.\tan\gamma_1.\tan\gamma_2) + K.(\tan\gamma_1 + \tan\gamma_2)/2}{I + \tan\gamma_1.\tan\gamma_2.J + G.(\tan\gamma_1 - \tan\gamma_2).\tan(\gamma_1 - \gamma_2) + K.(\tan\gamma_1 + \tan\gamma_2)/2}$$

The surface-deformation η is:

$$\eta = \frac{dF'}{dF''} = G$$

3.2. Numerical Results.

In order to obtain numerical results for TISSOT's τ, μ and η, the imaging equations were assumed to be:

$$\begin{aligned} x &= X_P \\ y &= (Y_P^2 + (Z_F - Z_P)^2)^{\frac{1}{2}} \end{aligned} \qquad (14)$$

Imaging equations (14) are obtained for x from formula (7c), where $v_F(t)$ is assumed to be a constant, and for y from formula (7a), by assuming $c_F / c'_m = \frac{1}{2}$ and $d_o = 0$. Thus there is an assumption made of perfect exterior orientation, straight and level flight. The object to be imaged is given by:

$$Z_P = Z_E - ((X_P - X_E)\cos\varepsilon + (Y_P - Y_E)\cos\delta)/\cos\vartheta$$

so that

$$x = X_P$$

$$y = (Y_P^2 + (Z_F - Z_E + ((X_P - X_E)\cos\varepsilon + (Y_P - Y_E)\cos\delta)/\cos\varphi)^2)^{\frac{1}{2}}$$

The object therefore is a plane through the point (X_E, Y_E, Z_E) and normal to the vector with direction cosines $(\cos\varepsilon, \cos\delta, \cos\varphi)$.

The differential quotients I, J, K, G result from the above imaging equations in a straight forward manner. Using these quotients to compute τ, μ and η, one gets tables 3, which are computed under the following assumptions: $X_P = Z_P = X_F = Y_F = X_E = Z_E = 0$, $Y_P = Y_E$; the object plane is parallel to the X-axis.

α (°)	γ_1 (°)	$\gamma_2 - \gamma_1$ (°)	Y_P (km)								
			5	10	20	5	10	20	5	10	20
0	0	22.5	-0.4	-0.1	0	-6.2	-2.2	-0.6	-12	-6.2	-2.2
		45	-0.6	-0.1	0	-9.8	-3.2	-0.9	-22	-9.8	-3.2
		67.5	-0.4	-0.1	0	-7.9	-2.4	-6.6	-21	-7.9	-2.4
	30	22.5	-0.1	0	0	-2.0	-0.4	-0.1	-6.8	-2.0	-0.4
		45	0.2	0	0	2.0	1.0	0.3	-0.4	2.0	1.0
		67.5	0.6	0.2	0	11	3.6	1.0	26	11	3.6
	60	22.5	0.3	0.1	0	6.2	2.0	0.5	14	6.2	2.0
		45	0.8	0.2	0	15	4.5	1.2	45	15	4.5
		67.5	1.0	0.3	0.1	20	6.0	1.6	56	20	6.0
10	0	22.5	-1.1	-0.5	-0.2	-9	-3.8	-1.5	-16	-9.0	-3.8
		45	-1.6	-0.6	-0.3	-15	-5.8	-2.2	-32	-15	-5.8
		67.5	-1.1	-0.5	-0.2	-13	-4.4	-1.6	-37	-13	-4.4
	30	22.5	-0.2	-0.1	0	-3.9	-1.0	-0.3	-11	-3.9	-9.7
		45	0.5	0.2	0.1	1.7	1.6	0.7	-7.3	1.7	16
		67.5	1.8	0.7	0.3	17	6.5	2.4	44	17	6.5
	60	22.5	1.0	0.4	0.2	9.6	3.6	1.3	17	9.6	3.6
		45	2.2	0.9	0.4	26	8.5	3.0	100	26	8.5
		67.5	2.9	1.2	0.5	33	11	4.0	120	33	11
30	0	22.5	-2.7	-1.3	-0.6	-16	-7.8	-3.5	-26	-16	-7.8
		45	-4.1	-1.8	-0.9	-31	-13	-5.3	-66	-31	-13
		67.5	-3.0	-1.3	-0.6	-35	-11	-4.0	-250	-35	-11
	30	22.5	-0.6	-0.2	-0.1	-11	-3.0	-0.9	-27	-11	-3
		45	1.3	0.6	0.3	-6.7	2.0	1.5	-89	-6.7	2
		67.5	4.5	2.1	1.0	42	14	5.9	-44	42	14
	60	22.5	2.5	1.1	0.5	17	8.1	3.3	-54	17	8.1
		45	5.7	2.6	1.2	97	21	7.8	-25	97	21
		67.5	7.4	3.4	1.6	120	27	10	-83	120	27
Z_P (km)			1			5			10		

(a)

Z_P (km)		1			5			10		
Y_P (km)		5	10	20	5	10	20	5	10	20
α (°)	0	0.98	1	1	0.71	0.89	0.97	0.45	0.71	0.89
	10	0.95	0.98	0.99	0.58	0.82	0.93	0.29	0.58	0.82
	20	0.91	0.96	0.98	0.45	0.73	0.88	0.12	0.45	0.73
	30	0.87	0.94	0.97	0.30	0.64	0.83	0	0.30	0.64

(b)

α (°)	β (°)	Z_P=1 km		Z_P=5 km		Z_P=10 km	
		Y_P=5 km	Y_P=20 km	Y_P=5 km	Y_P=20 km	Y_P=5 km	Y_P=20 km
0	30	1	1	0.94	0.99	0.89	0.97
	90	0.98	1	0.71	0.97	0.45	0.89
10	30	0.99	1	0.91	0.98	0.88	0.96
	90	0.95	0.99	0.58	0.93	0.29	0.82
20	30	0.98	0.99	0.89	0.97	0.87	0.94
	90	0.91	0.98	0.45	0.88	0.12	0.73
30	30	0.97	0.99	0.88	0.96	0.87	0.92
	90	0.87	0.97	0.30	0.83	0.07	0.64

(c)

Table 3.

Deformations according to TISSOT of (a) angles, (b) areas, (c) distances. It is assumed that the object plane is parallel to the flight line, and inclined with respect to the horizontal by an angle α, sothat $\varepsilon = 90^\circ$, $\delta = 90 + \alpha$, $\varphi = \alpha$. In table (a), γ_1 denotes the reference direction of an angle of size $\gamma_2 - \gamma_1$. In table (c), β is the angle between the flight direction and the distance.

Some important remarks about the numerical values should be pointed out:

The distance deformation factor τ can become very small and even negative, since a distance element in the object space can be imaged as a point or even inverted.

The factor μ , describing the deformation of angles, shows remarkably large values, especially for a plane being inclined for an angle of 30°, parallel to the flight line. This is, because the same can occur as with distances, namely imaging in an inverted position.

The area deformation η becomes extreme for a slope of 30° and for the surface element being located close to the flight track, namely half the flying height: There the surface dF" is shown in the imagery as a line, so that $\eta = 0$! Also here, negative values are possible for inverted slopes, but do not occur in the table.

To judge the numerical values in tables 3, one should bear in mind, that they are valid for only infinitesimally small units of the object space. Increasing the size of the elements for the definition of the deformations, one would find, that they are slightly larger, since the deformations reduce with distance from the flight track. Obviously, the deformations grow with flying height, reduced distance from the flight track, inclination of the object plane and increasing angle between the element and the flight direction.

4. DESCRIPTION OF METHODS FOR PLOTTING FROM A SINGLE STRIP OF SLAR-IMAGERY.

4.1. Introduction.

Generally, plotting from a single strip of imagery provides only planimetric coordinates as heights cannot be obtained. Thus, application of this approach should be limited to imagery from flat areas only. Only the use of an interferometer could extend the method in such a way, that all three model-coordinates are defined.

Since the projection parameters are varying from one image-point to another systematically as well as stochastically, meaningful plotting can be done by

- differential transformation of image into map coordinates by using the projection equations (1); these methods will be called "parametric";
- interpolation methods, in which image- and map coordinates are considered to be "inconsistent" in the sense of interpolation theory; these methods will be called "non-parametric", since they do not make use of the projection parameters;
- various combinations of parametric and non-parametric methods.

These methods can be applied in modes to be classified as:

- numerical
- photographical
- graphical.

4.2. Parametric Plotting.

4.2.1. General.

The parametric plotting consists of the use of the projection equations, such as (1). Resolution considerations lead to the conclusion that the vector $\Delta\underline{\bar{X}}$ can be neglected. Instead of geocentric coordinates, model coordinates are computed, so that matrix $\underline{D} = \underline{I}$. There appear 4 unknowns per 3 equations. So one unknown has to be assumed to be given. For the single strip of imagery-approach, this will be Z_P, which is assumed to be zero. So the algorithm is to compute $\mathfrak{Q}$ from the equation for Z_P and derive (X_P, Y_P) then from the two remaining projection equations.

This procedure is shorter than transforming equation (1) into:

$$(X - X_F)^2 + (Y - Y_F)^2 + (Z - Z_F)^2 - s^2 = 0$$

$$\frac{i_{11}(X - X_F)^2 + i_{12}(Y - Y_F)^2 + i_{13}(Z - Z_F)^2}{\left(\sum_{j=2}^{3} (i_{j1}\cdot(X-X_F) + i_{j2}(Y-Y_F) + i_{j3}(Z-Z_F)^2)^{\frac{1}{2}}\right.} = \tan \Phi_o, \quad \underline{I} = \underline{C}^T \cdot \underline{A}^T$$

as proposed by Rosenfield [51], and solving (X, Y) from the two non-linear equations by assuming $Z_P = 0$. Obviously, before applying the above algorithms, the slant ranges should, if necessary, be corrected for earth curvature and refraction.

If the elements of exterior orientation are not measured, there exists the theoretical possibility to compute them as unknowns from the projection equations by using a large number of control points. For this purpose, the exterior orientation could be assumed as piecewise linear function (see e.g. Masry [71]). Applying this to the equations (12), one would obtain:

$$\Delta x = \alpha_1 x + \alpha_2 y - \alpha_4 \sqrt{y^2 - Z_F^2} - \alpha_5 \cdot x \sqrt{y^2 - Z_F^2} + \alpha_6 + \alpha_7 x$$

$$\Delta y = \alpha_1 y - \alpha_2 x + \alpha_3 + \alpha_8 \cdot (y^2 - Z_F^2)^{\frac{1}{2}}/y + \alpha_9 \cdot x \cdot (y^2 - Z_F^2)^{\frac{1}{2}}/y +$$

$$+ \alpha_{10} Z_F/y + \alpha_{11} \cdot x \cdot Z_F/y \qquad (15)$$

The coefficients α_1, α_2, α_3 describe a general rotation, scale change and y-shift of the whole strip of imagery. The remaining coefficients change with the pieces of the imagery.

Along $x = x_{joint}$ one enforces

$$(\alpha_i + \alpha_{i+1} \cdot x)\ \text{piece}_j = (\alpha_i + \alpha_{i+1})\ \text{piece}_{j+1},$$

$$i = 2, 4, 6, 8, 10.$$

Instead of applying formula (15), in which the unknowns are computed with the help of control points, it is also possible to perform first a parametric transformation, to eliminate the systematic effect of viewing geometry and squint only (i.e. assuming exterior orientation to be ideal). Following that control points may be used for interpolation purposes.

4.2.2. Interpolation and Filtering of Exterior Orientation.

In the case where the exterior orientation is measured, a preliminary step in reducing the data should be undertaken. This step entails the elimination of the error of measurement, which is possible to a certain extent, using the methods developped in the theory of random functions. In the following, reference is made to section 2.2.2 on the stochastic model of exterior orientation.

The measurements of $\underline{f}(t)$ (the vector of the elements of exterior orientation) are erroneous. So, to use the proper values for the exterior orientation, the measured quantities have to be reduced for the error of measurement which has to be estimated; i.e. the measurements have to be "filtered".

The registration of the measurements $\underline{f}'(t)$ of the 6 components of $\underline{f}(t)$ can be discrete or continuous and analogue or digital. For numerical data handling, however, a digital, discrete form is required. For the digitization a certain interval Δt for the discrete measurements is to be chosen. One has to realize, that, in the frequency domain, all frequencies $> \frac{\pi}{\Delta t}$ are certainly lost. This critical frequency is also called "Nyquist-frequency" [66]. One has to choose it in a trade-off between numerical effort and accuracy. In this way, the components of the vector process $\underline{f}'(t)$ become stochastic sequences:

$$f_j'(t) = f_j'(t_i) \qquad \begin{matrix} i = 0, 1, 2, \ldots\ldots n \\ j = 1, 2, \ldots\ldots\ldots 6 \end{matrix}$$

The problem now is to estimate $\underline{f}(t)$, or better $\underline{g}(t)$, from the measured $\underline{f}'(t)$.

To this end, the mean $\underline{m}(t)$ has first to be subtracted from the measurements. Not going into the theory of aerodynamics to find a reasonably theoretically justified model, a flexible and general way is to eliminate $\underline{m}(t)$ with the help of a "moving average" (see Kendall [66], Yaglom [79]), a procedure which is very successful in its application to digital terrain models. In this, $m_j(t_i)$ is estimated as the weighted mean of a pregiven number of measurements $f_j(t_i - 1)$, $f_j(t_i - 2)$, ..., $f_j(t_i - n)$, $f_j(t_i + 1)$, $f_j(t_i + 2)$, ...$f_j(t_i + n)$. The weights are to be chosen in such a way, that the estimated $m_j(t_i)$ can be interpreted as the ordinate of a polynomial of order p:

$$m_j(t_i) = a_o + a_1 t_i + a_2 t_i^2 + \ldots\ldots\ldots a_p . t_i^p$$

at the abscissa $t_i = 0$. The parameter p defines the order of the moving average.

Figure 14 shows the example of recordings of the data of exterior orientation aboard a Transall C 160 in France, flying height approximately 8000 m, speed approximately 340 km/h.

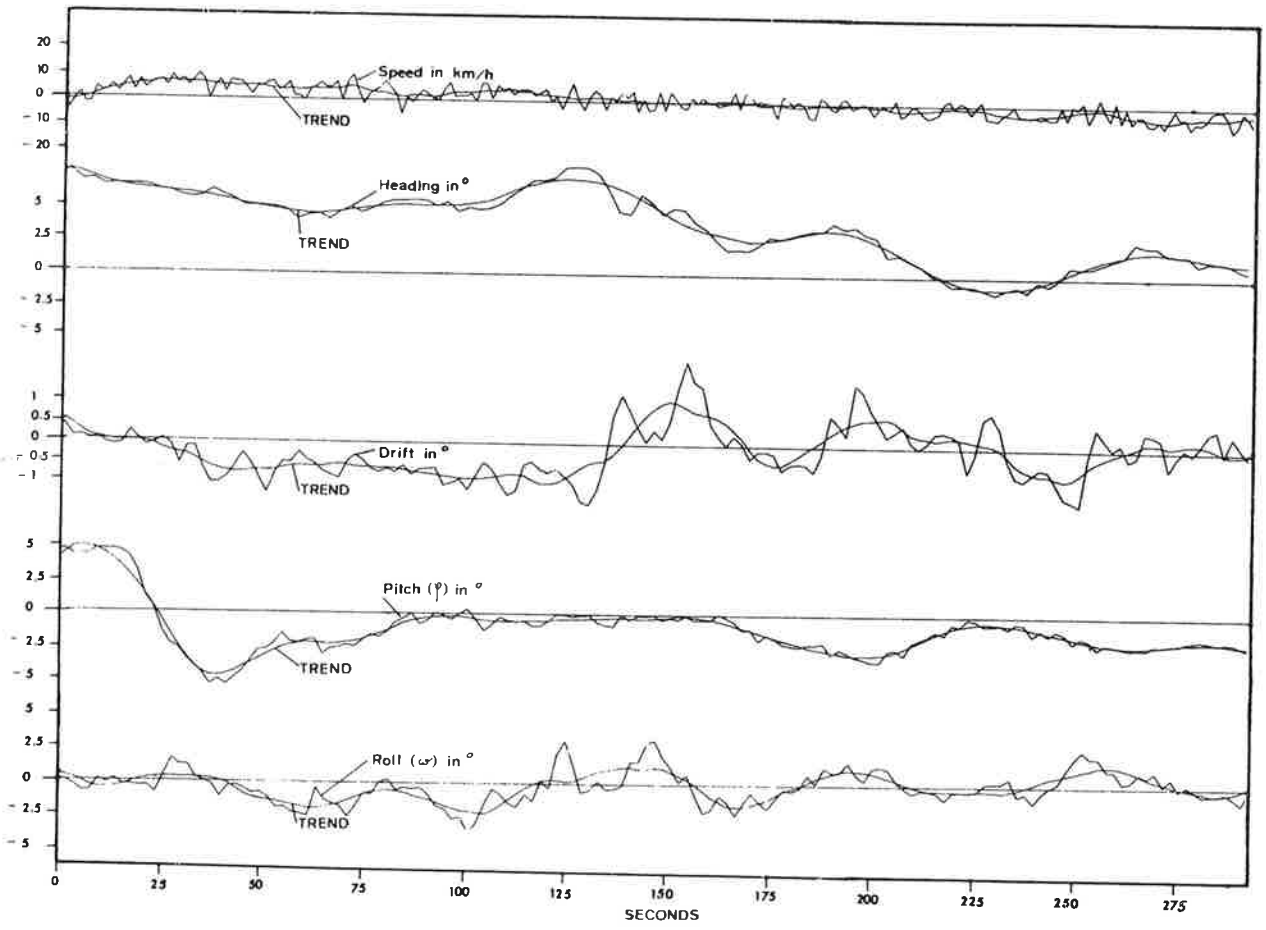

Fig. 14

Realization of exterior orientation, measured aboard a Transall C160; flying height ca. 8 km., speed ≈ 340 km/h. Trend computed by moving average of 3rd order, involving 17 points

These data have been made available by Prof. Ramsayer, University of Stuttgart. The trend is computed by means of a moving average of 3rd order, involving 17 points.

The residual stationary components $h_j(t_i)$ are then used to filter the "signal" $g_j(t_i)$. This is done with (N + 1) observed values of the

6 components in the equation

$$g_j(t_i - l.\,\Delta t) = \sum_{s=1}^{6} \sum_{k=0}^{N} a_{j,l,s,k} \cdot h_s(t_i - k.\,\Delta t) \quad (16)$$

representing a filter of Nth order.

The filter coefficients $a_{j,l,s,k}$ are unknown and have to be estimated in such a way, that the spur (or trace) of the correlation matrix of the filter errors is a minimum. This method is called "linear least squares interpolation and filtering":

$$sp(Cov) = \sum_{j=1}^{6} \sum_{l=0}^{N} E\{(g_j(t_i - l.\,\Delta t) \sum_{s=1}^{6} \sum_{k=0}^{N} a_{j,l,s,k} \cdot h_s(t_i - k.\,\Delta t))^2\} \quad (17)$$

The unknown $a_{j,l,s,k}$ can be solved from this equation system, if only the auto- and cross-correlation functions of $h_1, h_2 \ldots\ldots h_6$ (namely the q_{h_i, h_j}), of $e_1, e_2, \ldots\ldots e_6$ (namely the q_{e_i, e_j}) and their cross-correlation functions q_{h_i, e_j} would be known.

If now - as can reasonably be assumed - the $q_{h_i e_j}$ are all 0, then the following relation holds:

$$q_{g_i g_j} = q_{h_i h_j} - q_{e_i e_j} \quad (18)$$

The $q_{h_i h_j}$ can be computed from the given data, $\underline{h}(t_i)$, and the $q_{e_i e_j}$ must be found in a test of the measuring equipment. (The autocovariances of the data from fig. 14 are shown in fig . 15).

So from (17), the following system of equations results:

$$q_{g_i,g_j}((l-p).\,\Delta t) = \sum_{s=1}^{6} \sum_{k=0}^{N} a_{j,l,s,k} \cdot q_{h_s h_i}((k-p)\,\Delta t)$$

$$i,j = 1, 2, \ldots\ldots, 6$$

$$l,p = 0, 1, \ldots\ldots, N$$

These are $(N+1)^2 \cdot 1^2$ equations in the $(N+1)^2 \cdot 1^2$ unknown $a_{j,l,s,k}$.

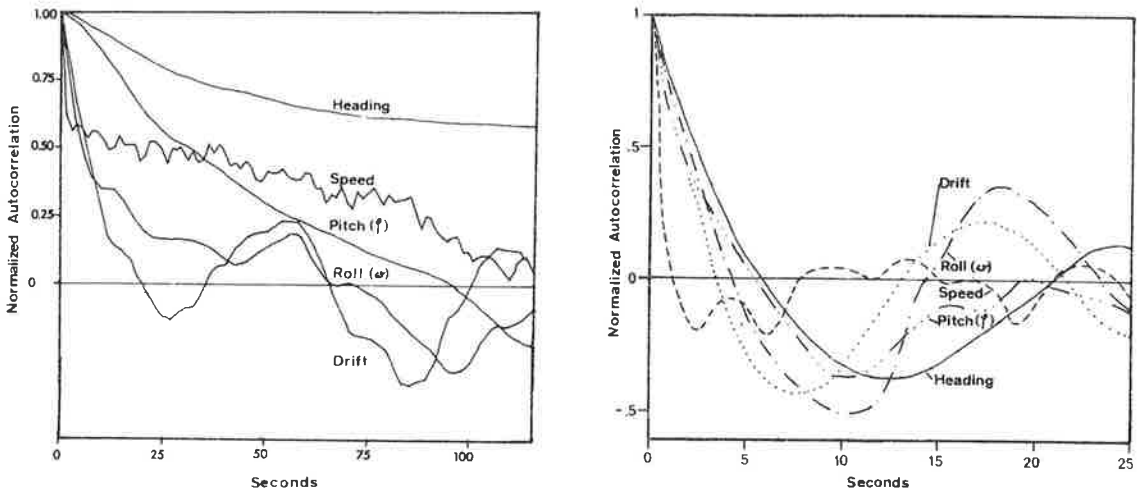

Fig. 15.

Autocorrelation of data in fig. 14, namely (a) of raw data and (b) of residuals after subtraction of trend.

The process consists of pure filtering, if a measurement was taken at the time $t_i - l.\Delta t$, (see formula 16). It consists of interpolation and filtering, if no measurement was given at time $t_i - l.\Delta t$. It consists of extrapolation (prediction) if $l < 0$.

In equation (18), the knowledge of $q_{e_i e_j}$ is required. As an alternative to find the covariances experimentally, Kraus and Mikhail are proposing, in e.g. [69] , to assume an uncorrelated measuring error, of which the covariance function is then singular:

$$q(\Delta t) = \sigma^2 \quad \text{for } \Delta t = 0$$

$$q(\Delta t) = 0 \quad \text{for } \Delta t \neq 0$$

In this special case, $q_{e_i e_j}$ is to be determined from the observations $\underline{h}$.

4.3. Non-Parametric, Interpolative Plotting.

Non-parametric plotting is based on the numerous methods of interpolation theory. Before applying one of these methods, the image coordinates have to be first transformed into the model system, e.g. by a parametric method under the assumption of ideal exterior orientation. There will then remain residual coordinate-discrepancies in given control points, to be interpreted as 2-dimensional stochastic fields. These are used to inter-

polate corrections in other points.

A group of powerful methods consists in the meshwise or piecewise interpolations, by which a continuous function is put through the residuals at the control (="reference"-) points.

In the piecewise bilinear interpolation a bilinear function is put through each group of three reference points (mesh), so that the residuals determine a polyhedron with plane, triangular pieces. The ambiguity of selecting triangles sometimes is overcome by constructing two networks of triangles. Each point to be transformed will then be within two triangles, so that an arithmetic mean has to be taken from the two results.

In general, however, any group of interpolation functions can be joined together. Numerically simple are the piecewise polynomials.

It is reasonable to establish polynomials which, in a way, describe the specific SLAR-residuals. For this it is to start from equation (12). By assuming flat terrain and polynomials of second order for the exterior orientation, one obtains:

$$\Delta x = -(a_0 + a_1 x + a_2 x^2) - y\,(1 - Z_F^2/y^2)^{\frac{1}{2}} \cdot (b_0 + b_1 x + b_2 x^2) - \\ - Z_F \cdot (c_0 + c_1 x + c_2 x^2)$$

$$\Delta y = -(1 - Z_F^2/y^2)\,(d_0 + d_1 x + d_2 x^2) + (e_0 + e_1 x + e_2 x^2) \cdot Z_F/y$$

From this results:

$$\Delta x = \alpha_0 + \alpha_1 x + \alpha_2 x^2 + \alpha_3 y + \alpha_4 xy + \alpha_5 x^2 y$$

$$\Delta y = \beta_0 + \beta_1 x + \beta_2 x^2 + \beta_3 y + \beta_4 y^2 + \beta_5 xy \qquad (20)$$

Forcing the polynomial pieces to have the same function value along a joining line $x = x_{const.}$, the joining conditions are:

$$(\alpha_0 + \alpha_1 x + \alpha_2 x^2)_{\text{piece } i} = (\alpha_0 + \alpha_1 x + \alpha_2 x^2)_{\text{piece } i+1}$$

$$(\alpha_3 + \alpha_4 x + \alpha_5 x^2)_{\text{piece } i} = (\alpha_3 + \alpha_4 x + \alpha_5 x^2)_{\text{piece } i+1}$$

$$(\beta_0 + \beta_1 x + \beta_2 x^2)_{\text{piece } i} = (\beta_0 + \beta_1 x + \beta_2 x^2)_{\text{piece } i+1}$$

$$(\beta_3 + \beta_4 x)_{\text{piece } i} = (\beta_3 + \beta_4 x)_{\text{piece } i+1}$$

$$(\beta_5)_{\text{piece } i} = (\beta_5)_{\text{piece } i+1}$$

Bosman et al. [4] recently proposed to extend the conditions imposed upon the polynomials by introducing a condition of minimum curvature. The algebraic solution of the problem becomes rather involved and demanding. The requirement for the minimum curvature, however, was felt due to the sometimes unfavourable behaviour of the polynomial pieces.

Simple nonparametric interpolation methods with one continuous function are a special case of the meshwise, since there is then only one single mesh for the whole interpolation area.

A second group of interpolation methods does not create a continuous function through the residuals at reference points, but only interpolates a group of discrete points (pointwise interpolation). The best known method is to interpolate a correction to a point by determining it as arithmetic or weighted mean of the neighbouring residuals.

The method of moving averages as described at the beginning of section 4.2.2. belongs to this group too.

A very powerful method is considered to be the linear least squares interpolation with known covariance matrix, a method also coming from the theory of stochastic processes. In this method the interpolation can be combined with filtering and has actually been described already above in section 4.2.2. on interpolation and filtering of data of exterior orientation. In the present application, the philosophy of this section 4.2.2. leads to the following algorithm:

$$\Delta x_i = \sum_{k=1}^{N} \sum_{j=1}^{N} q_j \cdot Q^{-1}_{kj} \quad x_k = \underline{q}^t \cdot \underline{Q}^{-1} \, \Delta \underline{x}$$

$\underline{q}$ is a vector of covariances between the value to be interpolated and the N reference points. $\underline{Q}$ is the matrix of covariances among the reference points. If filtering is applied, then $\underline{Q}$ consists of the covariances of the measurements, whereas $\underline{q}$ only contains the covariances of the signals. Thorough elaboration on this method is given at other occasions during this congress (Kraus & Mikhail [69]), so only a few remarks will be given:

This method of interpolation has optimum properties if the stochastic field, for which the entities to be interpolated are considered, is homogeneous.

This assumption is theoretically not fulfilled in the present application. Numerical studies will show up the difficulties when neglecting this condition of homogeneity.

4.4. Combination of Parametric and Non-Parametric Methods.

The combination of parametric and non-parametric methods is a most logical procedure to follow. The parametric method certainly will leave residual errors in the model coordinates, which by means of control points can be reduced by an interpolative process. An alternative would be, not to transform parametrically all points of interest, but only a limited number, forming e.g. a regular grid. By means of a non-parametric method then, the residual points are converted into the previously transformed network.

4.5. Numerical Plotting.

The method of numerical plotting is very flexible and computer-oriented. It consists of the measurement of image-coordinates, so that the relevant pictorial details are digitized, and subsequent digital transformation of these coordinates, mostly by means of a computing machine. The mathematical model used for the computation can be based on any of the previously described parametric or interpolative sets of formulae.

4.6. Photographic Plotting.

Partial or differential rectification only can allow a meaningful photographic plotting to be carried out. In [28] , a number of alternative solutions to the instrumental problem were enumerated. As the most promising was considered the differential electronic rectification, whose instrumental concept is shown in fig. 16. This concept seems to have been realized in the experimental Orthographic Radar Restitutor of the U.S. Department of Defense (see [11]).

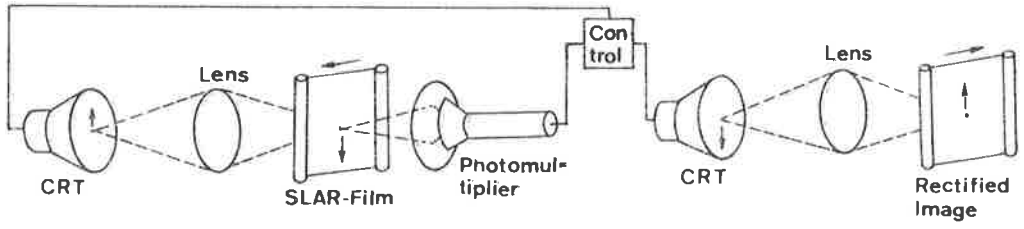

Fig. 16.
Electronic transformation of imagery.

The instrument settings must be given from either measurements of the data of exterior orientation or a previously performed numerical rectification. The flexibility of an electronic system as shown in fig. 16 would be advantageous especially in the case of differential rectification without a physical analog as after a non-parametric numerical rectification.

4.7. Graphical Plotting.

The numerical non-parametric methods do have graphical analogs. First there is the graphical interpolation after STRINZ. With this method, isolines are drawn trough the residuals in reference points by a human operator. From the isolines, corrections can be found to the coordinates of other points. Secondly it is possible to perform a graphical meshwise transformation using the well known paper strip method of projective geometry.

4.8. Numerical-graphical Plotting.

At present, plotting from single strips of SLAR-imagery is mostly done in a numerical-graphical way: a number of selected points is transformed numerically (mostly by a parametric method). This produces a grid of reference points. Using a method of partial rectification, the image-parts defined by the meshes of the grid are separately projected on the 4 grid points. The details are graphically traced. A photographic analogy is of course feasible as well. This method has been used to plot the maps of the Darien-province in Panama (see Hockeborn [16]).

Another concept would consist of connecting a sensing pen via a computer to a drawing table. Details from the imagery are traced by the sensor, transformed by the computer and drawn directly on the drawing-table. This concept is realized in the LR-1 line-rectifier of Bendix (Hattaway et al. [64]); its application to SLAR would, however, require an extension of the system.

5. NUMERICAL RESULTS.

5.1. Fictitious Imagery.

In the study [29], on which this report is based, numerical results after plotting from a single strip of imagery were obtained by using fictitious as well as actual imagery. Without going into the very involved problem of generating realistic fictitious SLAR-image coordinates, reference is made to fig. 17. From this figure conclusions can be drawn about the character of the plotting problem.

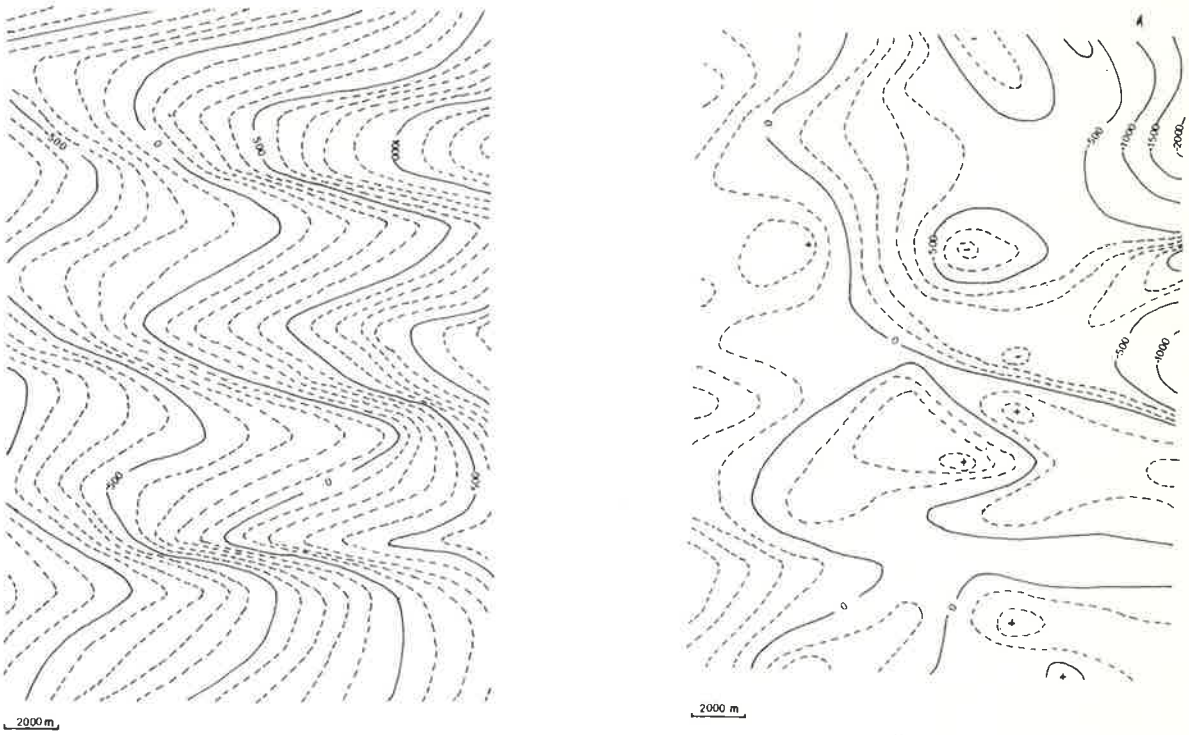

(a) Δx (b) Δy

Fig. 17.

Isolines through residual coordinate errors after linear conformal transformation of fictitious SLAR-imagery into map system.

In fig. 17 isolines are drawn through the Δx, Δy-residuals after a preliminary linear conformal transformation of fictitious SLAR-image coordinates into a reference system. As far as the absolute values of the residuals are concerned, it must be said, that the fictitious coordinates were generated under extreme assumptions for the terrain-

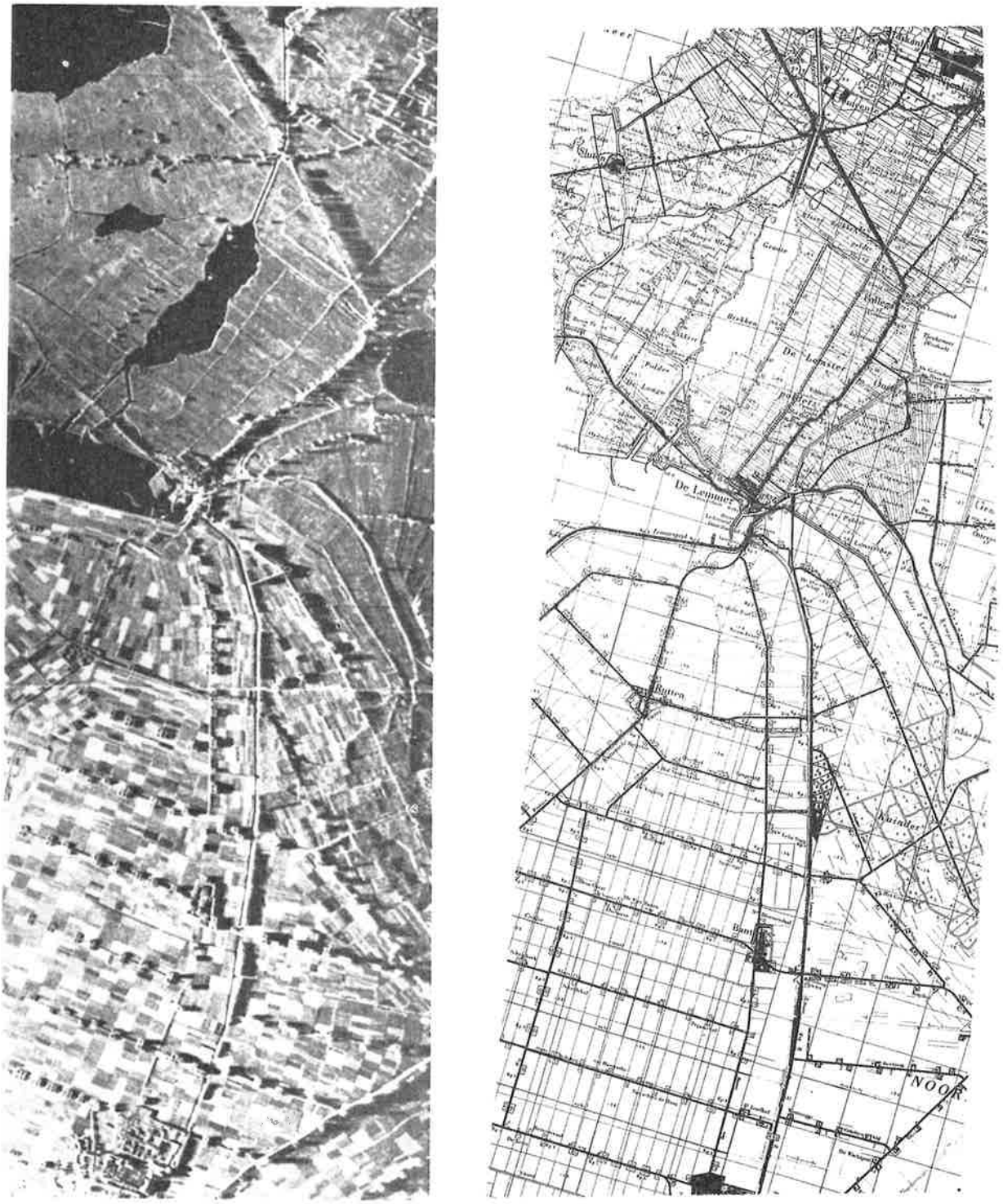

Fig. 18.

Sample of SLAR-imagery and map 1 : 50 000 of Noordoostpolder, Netherlands, at scale ≈ 1 : 125 000.

relief, the errors of exterior orientation and the flying height.

Fig. 17a. shows distinctly the stochastic anisotropy of Δx: correlation of coordinate errors is different in x- and y-directions. It becomes obvious, that perimeter-control only could already well describe the Δx-residuals: only the two edges of the imaged area parallel to the flight line must be controlled. The required density of this collinear arrangement of control depends on the behaviour of the exterior orientation elements. Assuming that along a flight line the deviations of the exterior orientation from the ideal are decomposed into a Fourier-series, then with a mean "bridging distance" x between control points, the minimum wavelength of the (errors of) exterior orientation to be taken care of is $\lambda = 2. x$.

Fig. 17b. makes it obvious that the Δy are mainly a function of terrain relief. The proper distribution of control points consists of a good description of the height differences, so that the problem is similar to the one in conventional partial photogrammetric rectification.

5.2. Actual Imagery.

To test the non-parametric methods of numerical plotting, a strip of actual SLAR-imagery was used, which is shown in figure 18, together with a map of the same area. The imagery was flown by the British Royal Radar Establishment over the North-East-Polder in the Netherlands, at a flying height of less than 200 m. There was no further information whatsoever available on the imagery.

In an area of approx. 10 x 20 kms^2 the coordinates of 159 points were measured on the SLAR-imagery as well as on the map. The measuring instrument was the WILD-A10 of the Geodetic Institute in Delft because of the registring equipment EK 8 that is connected to it.

The lack of any information on the type of representation and exterior orientation did not allow any parametric transformation to be applied to the image-coordinates. The residual error vectors as shown in fig. 19 resulted in the 159 points after a linear conformal transformation. After choosing 20 reference points evenly distributed over the area, various interpolation methods were applied to reduce the residuals. The result of these efforts is shown in table 4.

The vector diagram of fig. 19 shows a marked change in the statistical properties of the residuals in the last third of the strip. In terms of the theory of random functions, the field is definitely inhomogeneous. This means than an approach via piecewise methods seems reasonable. This is

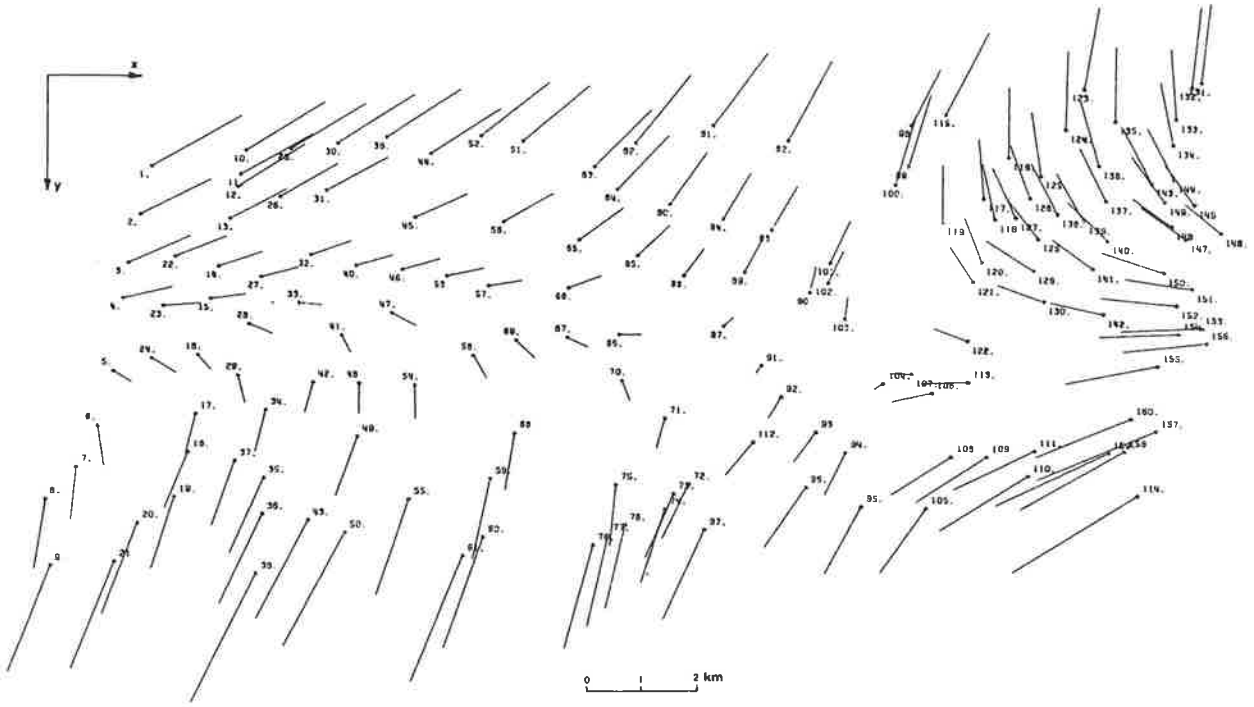

Fig. 19.

Error vectors after linear conformal transformation of SLAR coordinates, measured in the imagery of fig. 18. (Error vectors exaggerated 3 times).

	Zone	ORT	MIT	INT	AFT	AFT mitt.	POL	AEU	Strinz
σ_x	I	271	73	45	84	65	62	56	54
	II	266	62	56	79	60	**51**	62	53
	III	275	87	85	62	42	37	84	52
	IV	249	114	91	37	38	43	95	74
σ_y	I	348	**48**	43	36	32	28	68	45
	II	184	76	42	28	29	16	74	35
	III	199	79	90	32	23	21	52	38
	IV	516	115	87	38	42	24	56	47

Table 4.

Result of the transformation of SLAR-image coordinates into map system. SLAR-imagery shown in fig. 18. Values in m on the ground. Four zones parallel to the flight line. ORT = linear conformal transformation; MIT = arithmetic mean; INT = linear least squares interpolation; AFT = meshwise linear interpolation; AFT_{mitt} = every point transformed in two meshes with AFT, then arithmetic mean taken; POL = piecewise polynomial (formula (20)); AEU = transformation according to formula (19).

verified by table 4, in which the piecewise polynomial (POL) as given in formula (20), and the meshwise bilinear transformation (AFT), bring the best results. The presentation of the results is for 4 zones parallel to the flight line, since there are variations of the r.m.s. errors to be expected.

The method of linear least squares interpolation (INT) was unsatisfactory, at least in its straight forward application with a pregiven normalized covariance function

$$\text{Cov}\ (t) = 1\ /\ (1 + t/t_o)^2$$

in which t is the distance between two points and t_o an (experimentally optimized) constant of 20 km. This approach does not allow filtering of an uncorrelated component.

Normalized covariance functions have also been computed from the measurements, such as to allow filtering of an uncorrelated component. From 40 reference points it was obtained:

$$\text{Cov}_{\Delta x}\ (t) = 0.95\ \bar{e}^{.002.t}$$

$$\text{Cov}_{\Delta y}\ (t) = 0.50\ \bar{e}^{.00016.t}$$

Application of these covariance functions to least squares interpolation and filtering from 20 reference points results in:

$$\sigma x = \pm 55\ \text{m} \qquad \sigma y = \pm 101\ \text{m}$$

This result is, for Δ y, significantly inferior to other methods. The reason seems to be that the covariance function is not well defined, due to the inhomogeneity and anisotropy of the data.

To prove the conclusion on perimeter control, which was drawn from fig. 17a, the graphical method of STRINZ was repeated for 20 reference points, this time aligned along the edge of the imaged area. Table 5 shows the marked improvement in x with this type of distribution of control. The residual errors are of the order of magnitude of the resolution capacity of the SLAR-system in question.

Zone	I	II	III	IV
σ_x	28	34	34	33

Table 5.

σ_x after graphical interpolation with perimeter control only.

A similar experiment with plotting from single strips of imagery was performed by NIWARS, in Delft, the Netherlands [4], and at the University of Hannover, W.-Germany. In the first example, 3 strips of SLAR-imagery were transformed into the map system, using a meshwise bicubic transformation with the condition of minimum curvature. The results are given in table 6, converted to metres on the ground to allow for easier comparison with tables 4 and 5. It is not possible to draw significant conclusions about the interpolation method, since the strips of imagery may not compare at all concerning the circumstances under which they were taken. These circumstances, however, do influence the Δx. As regards the results from Hannover, reference has to be made to the paper by Konecny [22].

Image scale	σ_x(m)	σ_y(m)	Flight height (m)
1 : 250.000	47.5	45	150
1 : 250.000	47.5	60	150
1 : 420.000	80	46	4500

Table 6.

Standard deviation of transformed coordinates in three strips of SLAR-imagery of flat area (Netherlands) (from Bosman et al. [4]).

5. CONCLUSIONS AND RECOMMENDATIONS.

5.1. Conclusions.

Due to their unique all-weather capability and active mode of operation, side-looking radar sensors are of growing importance to photogrammetry: airborne data acquisition for subsequent production of topographic and thematic maps, as made possible by these systems, is especially useful, when the alternative of conventional photography is not possible.

The vector $\underline{s}$ between the antenna and the object point - as given in the reference (ground-) coordinate system - is transformed by the projection equation into an antenna coordinate system. Consideration of the earth's ellipsoidical reference figure leads to the conclusion, that only its spherical shape is of significant importance for the vector $\underline{s}$, whereas the eccentricity is negligible, as is the effect of refraction due to the atmosphere's variable index of refraction.

The erroneous exterior orientation of the antenna propagates into the length of the vector $\underline{s}$ only with errors in position. Erroneous attitude is of no significance for the length of $\underline{s}$, but for the time a given object point is imaged. Since the x-image coordinates in a SLAR-strip (in flight direction) are functions of time, attitude is relevant for x-image coordinates. Position of the sensor is significant for the y-image coordinates (across flight direction).

The stochastic model of SLAR involves the concept of random functions. The elements of exterior orientation especially, can be statistically described by their auto- and cross- covariance functions. Applying the law of propagation of covariances, one obtains the stochastic model of image coordinates. It turns out, that the image-displacements due to errors in exterior orientation are inhomogeneous and anisotropic in the statistical sense.

The numerical results obtained from TISSOT's theory to describe the characteristic properties of the SLAR projection quantitatively verify the increase in the deformation of various entities, such as angles, distances, and areas, with increasing flying height and reduced ground range.

It is possible to classify the methods of plotting from a single strip of SLAR-imagery as parametric or interpolative, the first making use of

the projection equations, the latter considering the image- and ground-coordinates just as "inconsistent" in the sense of interpolation theory. The most effective approach seems to be a combination of both: first a parametric transformation is performed. Eventual residual errors in control points can then be reduced by an interpolative method.

The numerical results obtained from a strip of SLAR-imagery of the Netherlands, however, concern the purely interpolative approach, since no parameters of the projection equation were known. A comparison of the various interpolation methods shows, that the piecewise polynomial performs more favourably than the other methods, in particular the pointwise. This may lead to the conclusion, that the pointwise interpolation methods are very sensitive to conditions to be fulfilled by the data, namely stochastic homogenity and isotropy, which do not apply for SLAR. So the r.m.s. errors after transformation, as found from check points in metres on the ground, vary from $\pm$ 20 m to $\pm$ 60 m in y, and $\pm$ 30 m to $\pm$ 80 m in x, according to various strips of imagery, methods of plotting and distribution of control.

6.2. Recommendations.

There are of course a number of unsolved problems of varying priority which at this occasion should be brought forward. In the first place there is a definite lack of information on the sensors themselves. This, to a certain extent, hampers the success of efforts to popularize the concept of mapping with SLAR among the photogrammetric community. Efforts should therefore be undertaken to make on the one hand the state of the art available for civil use and on the other hand, not to monopolize it to the extent as presently experienced.

Another point of vivid interest is the interferometric method of measuring the depression angle Ω with SLAR-systems. The concept has a very attractive feature in the fact that an automatic on-line map production is made feasible. The signals for the slant ranges and depression angle Ω are present as electric analogues, so that computerization - even in flight - is favoured. It is to be assumed that on this particular aspect more is to be contributed by presentation from the side of Commission II.

Furthermore a larger number of controlled practical experiments should become possible, e.g. by making available to appropriate, preferably non-profit institutions, the required material, such as imagery, auxiliary data and control information.

A final remark then still concerns the initiative to be taken by Commission IV in the direction of mapping from side-looking-radar. A need exists to establish procedures as well as accuracy models for the preparation of, on one hand, SLAR-mosaics and base maps for thematic mapping and, on the other hand, topographic maps from SLAR. It is recommended to give these problems priority from the side of Commission IV.

Acknowledgement.

I wish to express my sincere gratitude to the management of ITC, Enschede, for the support in the course of this study. I am grateful to Prof. Dr. K. Ramsayer, Stuttgart, Germany, for the sample of navigational data in figure 14; to Dr. K. Kraus, Stuttgart, for running the data in section 5 with his program for least squares interpolation; to Mr. K. Tempfli for some assistance in programming for section 5, and finally to Prof. Dr. E.M. Mikhail, for discussion and valuable assistance in the course of preparing this report.

BIBLIOGRAPHY ON MAPPING FROM SLAR .

1. AKOWETZKI, W.I. "On the Transformation of Radar Coordinates into the Geodetic System", Geodesia i Aerofotosjomka, 1968, in Russian.

2. AMBROSE, W. "A Radar Image Correlation Viewer", Phot. Eng., Vol. XXXIII, 1967.

3. ANONYMOUS. "Westinghouse Earth Resources SLAR Mapping System ER 3", Westinghouse Electric Corp. Techn. Publ. No. 9724a, Baltimore, U.S.A.

4. BOSMAN, E., CLERICI, E., ECKHARDT, D., KUBIK, K. "Project Karaka - The Transformation of Points from Side Looking Radar Images into the Map System", Final Report, Part I, NIWARS, Delft, Netherlands, 1971.

5. CLAVELOUX, B.A. "Sketching Projector for Side-looking Radar Photography", Phot. Eng., Vol. XXVI, 1960.

6. CRANDALL, C.J. "Advanced Radar Map Compilation Equipment", Phot. Eng., Vol. XXIX, 1963.

7. CRANDALL, C.J. "Radar Mapping in Panama", Phot. Eng., Vol. XXXV, 1969.

8. DALKE, G., McCOY, R. "Regional Slopes with Non-Stereo Radar", Phot. Eng., Vol. XXXV, 1968.

9. DERENYI, E.E. "Relative Orientation of Continuous Strip Imagery", Univ. of New Brunswick, Ph.D.-Thesis, Canada, 1970.

10. DI CARLO, C., CRANDALL, C.J. "All Weather Mapping", Presented Paper, FIG-Congress , 1968.

11. DI CARLO, C., DE METER, E.R. "DoD Data Processing Equipment for Radar Imagery", Presented Paper, FIG-Congress in Wiesbaden, Germany, 1971.

12. ESTEN, R.D. "Radar Relief Displacement and Radar Parallax", USAERDL-Report No. 1294, Ft. Belvoir, USA, 1953.

13. FIORE, C. "Side-Looking Radar Restitution", Phot. Eng., Vol. XXXIII, 1967.

14. GEIER, F. "Beitrag zur Geometrie des Radarbildes", Ph.D. Thesis, Techn. Univ. of Graz, Austria, 1971.

15. HEMPENIUS, S.A. "Image Formation Techniques for Remote-Sensing from a Moving Platform", ITC-Publ. Serie A, No. 46, 1969.

16. HOCKEBORN, H.A. "Extraction of Positional Information from Side Looking Radar", Presented Paper ISP-Comm. II - Symp., Munich, 1970.

17. HOFFMANN, P. "Photogrammetric Applications of Radar-Scope Photographs", Phot. Eng., Vol. XXIV, 1958.

18. HOHENBERG, F. "Zur Geometrie des Funkmessbildes", Austrian Academy of Sciences, Math.-Naturwiss. Klasse, Volume 2-3, 1950.

19. KOBER, C.L., SIEFKER, R.G. "Determination of Target Height from Radar PPI Photographs", Airforce Techn. Report No. 6500, Wright Air Development Centre, Ohio, 1950.

20. KONECNY, G. "Metric Problems in Remote Sensing", Proceed..of the ISP Comm. IV Symp., Delft, 1970, ITC Publ. Series A, No. 50.

21. KONECNY, G. "Orientierungsfragen bei Streifenbildern und Aufnahmen der Infrarotabtastung", Presented Paper, ISP-Comm. II Symp., Munich, 1970.

22. KONECNY, G. "Geometrical Aspects of Remote Sensing", Invited Paper, ISP-Congress, Ottawa 1972.

23. KONECNY, G., DERENYI, E.E. "Geometric Considerations for Mapping from Scan Imagery", 4th Symp. on Remote Sensing, Univ. Of Michigan; Ann-Arbor, USA, 1966.

24. LA PRADE, G.L. "An Analytical and Experimental Study of Stereo for Radar", Phot. Eng., Vol. XXIX, 1963.

25. LA PRADE, G.L. "Subjective Considerations for StereoRadar", Goodyear Aerospace Corp., GiB-9169, 1970.

26. LA PRADE, G.L., LEONARDO, E.S. "Elevations from Radar Imagery", Phot. Eng., Vol. XXXV, 1969.

27. LEBERL, F. "Metric Properties of Imagery Produced by Sidelooking Airborne Radar and Infrared Line Scan Systems", Proced. of the ISP Comm.IV Symp., Delft, 1970, ITC Publ. Series A, No. 50.

28. LEBERL, F. "Vorschläge zur intrumentellen Entzerrung von Abbildungen mit Seitwärts Radar (SLAR) und Infrarotabtastsystemen (IRLS)", Bild-messung und Luftbildwesen 1971/2.

29. LEBERL, F. "Untersuchung über die Geometrie und Einzel-bildauswertung von Radarschrägaufnahmen", Ph.D.-Thesis, Techn. Univ. Vienna, Austria , 1971.

30. LEBERL, F. "Remote-Sensing, Neue Entwicklungen zur Wahrnehmung auf Abstand", Österreichische Zeitschrift für Vermessungswesen, 1971/6.

31. LEBERL, F. "On Model Formation with Remote Sensing Imagery", Special issue for ISP-Congress 1972 of the Österreichische Zeitschrift für Vermessungswesen, 1972.

32. LEONARDO, E.S. "An Application of Photogrammetry to Radar Research", Phot. Eng., Vol. XXV, 1959.

33. LEONARDO, E.S. "Comparison of Imaging Geometry for Radar and Photographs", Phot. Eng., Vol. XXIX, 1963.

34. LEONARDO, E.S. "Capabilities and Limitations of Remote Sensors", Phot. Eng., Vol. XXX, 1964.

35. LEONARDO, E.S. "Reliability of Remote Sensing Imagery", Phot. Eng., Vol. XXXI, 1965.

36. LEVINE, D. "Radargrammetry", McGraw Hill Book Comp., 1960.

37. LEVINE, D. "Principles of Stereoscopic Instrumentation for PPI-Photography", Phot. Eng., Vol. XXX, 1963.

38. LEVINE, G. "Automatic Production of Contour Maps from Radar Interferometric Data", Semi Annual ASP-Convention, Dayton, Ohio, 1965.

39. LOELKES, G.L. "Radar Mapping Imagery - Its Enhancements and Extraction for Map Construction", Semi-Annual ASP-Convention, Dayton, Ohio, 1965.

40. LOOR, G.P. de "Possibilities and Uses of Radar and Thermal Infrared Systems", Photogrammetria, Vol. 24, 1969.

41. MACCHIA, R.P. "Radar Presentation Restitutor", Phot. Eng., Vol. XXIII, 1957.

42. MANUAL OF PHOTOGRAMMETRY "Photogrammetric and Radargrammetric Techniques", Vol. II, 3rd. Edition, 1966.

43. MIRANDA, A. "Radar Stereo Equipment", Goodyear Aerospace Corp., GiB - 9198, 1970.

44. MOORE, R.K. "Heights from Simultaneous Radar and Infrared", Phot. Eng., Vol. XXXV, 1969.

45. NIMS, A.A. "All-Weather Mapping by Radar", Westinghouse Engineer, 1968.

46. NORVELLE, F. Raye. "AS-11-A Radar Program", Phot. Eng., Vol. XXXVIII, 1972.

47. ORLANDO, C. "Tactical Image Interpretation Facility", Phot. Eng., Vol. XXXIII, 1967.

48. PROTHEROE, W.M., DICKEY, F.P. "The Geometry of the Radarscape", Techn. Paper No. 107, Mapping and Charting Lab., Ohio State Univ., 1950.

49. RINNER, K. "Die Geometrie des Funkmessbildes", Austrian Academy of Sciences, Math.-Naturw. Klasse, 1948.

50. RINNER, K, BENZ, F. "Handbuch der Vermessungskunde", Jordan-Eggert-Kneissl, Vol. II, Metzlersche Verlagsbuchhandlung, Stuttgart, 1966.

51. ROSENFIELD, G.H. "Stereo Radar Techniques", Phot. Eng., Vol. XXXIV, 1968.

52. SCHEPS, B.B. "To Measure is to Know - Geometric Fidelity and Interpretation in Radar Mapping", Phot. Eng., Vol. XXVI, 1960.

53. SCHREITER, J.B. "Strip Projection for Radar Charting", Techn. Paper No. 130, Mapping and Charting Lab., Ohio State Univ., 1950.

54. SINGLETON, R.R. "Projection for Line Scan Recording Devices", Techn. Paper No. 178, Mapping and Charting Lab., Ohio State Univ., 1953.

55. SMITH, H.P. "Mapping by Radar - The Procedures and Possibilities of a New and Revolutionary Method of Mapping and Charting", USAF, Randolph Field, Texas, 1948.

56. STILWELL, J.E. "Radar Network Adjustment", Phot. Eng., Vol. XXIX, 1963.

57. TOMANN, G.C., "Acoustic Simulation of Stereo Radar", Tech. Item Nr. 133-8, CRES, Univ. of Kansas, Lawrence, USA, 1969.

58. YORITOMO, K. "All Weather Mapping", Semi Annual ASP Convention, Dayton, Ohio, 1965.

59. YORITOMO, K. "Radar as a Mapping Sensor", Ft. Belvoir, Virginia, USA.

60. YORITOMO, K. "Comparisons of Photogrammetric and Radar Data Reduction", Ft. Belvoir, Virginia, USA.

RELATED LITERATURE AND REFERENCES

61. CASE, J.B. "The Analytic Reduction of Panoramic and Strip Photography", Photogrammetria 1967.

62. CUTRONA, J.L. "Synthetic Aperture Radar", in "Radar Handbook", McGraw Hill, New York, 1962.

63. ELMS, D.G. "Mapping with a Strip Camera", Phot. Eng., Vol. XXVIII, 1962.

64. HATTAWAY, D.P. et al. "A New Portable Line Rectifier", Bendix Research Lab., Southfield, USA, 1970.

65. JONES, F.A. "Geometric Analysis of Airborne Infrared Terrain Maps", Semi Annual ASP-Convention, Dayton, Ohio, 1965.

66. KENDALL, M.G., STUART, A. "The Advanced Theory of Statistics", Vol. 3., Chapter 45-50, Griffin & Co., London, 1966.

67. KONECNY, G., DERENYI, E.E. "Geometry of Infrared Imagery", Can. Surveyor, 1964.

68. KONECNY, G., DERENYI, E.E. "Infrared Scan Geometry", Phot. Eng., Vol. XXXIII, 1966.

69. KRAUS, K., MIKHAIL, E.M. "Linear Least Squares Interpolation and Filtering in Computational Photogrammetry", Presented Paper, Comm. III, ISP-Congress, Ottawa, 1972.

70. LAURILA, S. "On the Shoran Photogrammetric Position Fixing", Photogrammetria 1954/55, No. 4.

71. MASRY, S.E. "Analytical Treatment of Stereo Strip Photos", Phot. Eng., Vol. XXXV, 1969.

72. OCKERT, D. "Satellite Photography with Strip- and Frame Cameras", Phot. Eng., Vol. XXVI, 1960.

73. SCHATZ, U. "Das Problem der optimalen Stützpunktdichte und der optimalen Maschengrösse bei Transformationen ungleichartiger Koordinaten", Ph.D. Thesis, Univ. of Bonn, W. Germany, 1970.

74. SHERSHEN, A.I. "Aerial Photography", Moskow, 1958. Translated by Israel Program of Scientific Translations, Jerusalem, 1962.

75. TAYLOR, J.I. "Rectification Equations for Infrared Line-Scan Imagery", Proceed. of the ISP-Comm. IV-Symp., Delft, 1970, ITC-Publ. Series A, No. 50.

76. TISSOT, M.A. "Mémoire sur la Représentation des Surfaces", Gautier-Villars, Paris, 1881.

77. WOLF, H. "Ausgleichsrechnung nach der Methode der kleinsten Quadrate", Dümmler Verlag, Bonn, W. Germany, 1968.

78. WONG, K.W. "Geometric Calibration of Television Systems for Photogrammetric Applications", Presented Paper, ISP-Congress, Lausanne, 1968.

79. YAGLOM, A.M. "Introduction to the Theory of Stationary Random Functions", Prentice Hall Inc., 1962.